NANOMATERIALS

Carbon-based electrocatalysts for advanced energy conversion and storage

10.1126/sciadv.1500564

Jintao Zhang,[1]* Zhenhai Xia,[2] Liming Dai[1]†

Oxygen reduction reaction (ORR) and oxygen evolution reaction (OER) play curial roles in electrochemical energy conversion and storage, including fuel cells and metal-air batteries. Having rich multidimensional nanoarchitectures [for example, zero-dimensional (0D) fullerenes, 1D carbon nanotubes, 2D graphene, and 3D graphite] with tunable electronic and surface characteristics, various carbon nanomaterials have been demonstrated to act as efficient metal-free electrocatalysts for ORR and OER in fuel cells and batteries. We present a critical review on the recent advances in carbon-based metal-free catalysts for fuel cells and metal-air batteries, and discuss the perspectives and challenges in this rapidly developing field of practical significance.

INTRODUCTION

With diminishing fossil fuels, increasing demand on energy resources, and growing environmental concerns, the development of clean and sustainable energy conversion and storage systems with a high efficiency and low cost, such as fuel cells and metal-air batteries, has become more important than ever (*1*). However, implementing these energy technologies in our daily life is still a big challenge because catalysts are required for oxygen reduction reaction (ORR) in fuel cells and for both ORR and oxygen evolution reaction (OER) in rechargeable metal-air batteries (*2*). Traditionally, platinum supported on carbons (Pt/C) has been regarded as the best catalyst for ORR, although it still suffers from multiple drawbacks, including its susceptibility to time-dependent drift, fuel crossover, and CO poisoning effects (*3*, *4*). On the other hand, metal oxides (for example, RuO_2, MnO_2, and perovskite oxides) have been widely explored as electrocatalysts for OER (*5*). However, the high cost and poor durability of noble metal/metal oxide catalysts have precluded the commercialization of fuel cell and metal-air battery technologies (*6*). Therefore, the large-scale practical application of fuel cells and metal-air batteries cannot be achieved unless the expensive noble metal (for example, platinum)/metal oxide electrocatalysts for ORR/OER are replaced by other efficient, low-cost, and durable electrode materials.

Along with the intensive research efforts in developing nonprecious metal catalysts to reduce or replace noble metal catalysts for clean and renewable energy technologies, we have discovered a new class of low-cost, metal-free ORR catalysts based on nitrogen (N)–doped carbon nanotubes (NCNTs), which performed better than platinum in alkaline fuel cells (*7*). The improved catalytic performance for the NCNTs can be attributed to the electron-accepting ability of the nitrogen atoms, which creates net positive charge density on adjacent carbon atoms in the nanocarbon structure for changing the oxygen adsorption mode to facilitate ORR (*8*). Subsequent research activities carried out in many laboratories worldwide, including our own, have not only confirmed the above findings but also provided further support for the important role of doping-induced charge transfer in the design and development of new metal-free catalytic materials for fuel cells and metal-air batteries (*9*–*16*). It was further demonstrated that not only did those carbon nanomaterials [for example, one-dimensional (1D) CNTs and 2D graphene] doped/co-doped by various heteroatoms (for example, N, B, P, S, Br, Cl, and I) exhibit high ORR (*17*–*22*), but undoped carbon nanomaterials adsorbed with polyelectrolytes also showed high ORR catalytic activities through intermolecular charge transfer (*23*, *24*). We have also recently demonstrated that metal-free NCNTs and their graphene composites with porous structures perform better and are more durable than the state-of-the-art nonprecious iron–based catalyst even in acidic polymer electrolyte membrane fuel cells (PEMFCs) (*25*)—the mainstream fuel cell technology. Furthermore, recent papers (including those by our group) have reported that carbon nanomaterials can act as either monofunctional or bifunctional metal-free catalysts for ORR, OER, hydrogen evolution reaction (HER), carbon dioxide reduction (CDR), and even triiodide to iodide reduction—reactions crucial to fuel cells, metal-air batteries, water splitting for fuel generation, and dye-sensitized solar cells (DSSCs) (*26*–*33*). Among them, 3D carbon nanoarchitectures with well-defined porous network structures and large surface/interface areas for a high density of active centers and efficient electron/electrolyte transports are of particular interest for high-performance electrolysis (*34*). These studies represent major breakthroughs in the emerging field of carbon-based metal-free catalysts (*34*–*36*), which will remove the bottlenecks to translating low-cost, metal-free, carbon-based catalysts to commercial reality, and open avenues for clean energy generation and storage with affordable and durable fuel cells and metal-air batteries. The widespread use of carbon-based metal-free catalysts will surely result in better fuel economy, lower harmful emissions, and less reliance on petroleum sources. This could markedly improve our daily life in the near future. Because so many carbon-based catalysts, along with the related theoretical work, have recently been reported, this once emerging field has grown to a critical point for a timely summary of the fruitful achievements and a critical outlook for future development. This article aims to provide a critical review of the recent progresses, along with perspectives and challenges, in this fast-growing field of great significance.

EVALUATION OF ELECTROCATALYTIC ACTIVITY TOWARD ORR AND OER

In principle, oxygen reduction can occur in both alkaline and acidic media either through a two-electron transfer process to produce peroxide

[1]Center of Advanced Science and Engineering for Carbon (Case4Carbon), Department of Macromolecular Science and Engineering, Case Western Reserve University, Cleveland, OH 44106, USA. [2]Department of Materials Science and Engineering, Department of Chemistry, University of North Texas, Denton, TX 76203, USA.
*Present address: Key Laboratory of Colloid and Interface Chemistry, Ministry of Education, School of Chemistry and Chemical Engineering, Shandong University, Jinan 250100, China.
†Corresponding author. E-mail: liming.dai@case.edu

species as an intermediate, followed by further reduction to OH^-/water, or through a more efficient four-electron transfer to directly produce H_2O as the only by-product (Scheme 1) (*37*):

To evaluate the electrocatalytic activity of catalysts for ORR in aqueous electrolytes, the most commonly used techniques include rotating disc electrode (RDE), rotating ring-disc electrode (RRDE), linear scan voltammetry (LSV), and steady-state polarization (*38*). The overall measured ORR current (J) is dependent on the kinetic current (J_k) and diffusion-limiting current (J_d), as shown in Eq. 1. J_k is determined by the reaction kinetic process. If the applied overpotential is high enough, however, every atom/ion reaching the electrode reacts immediately; thus, the reactant (for example, O_2) concentration at the electrode surface becomes nearly zero, leading to a diffusion-limiting current (that is, J_d). J_d is only determined by the rate of diffusion. Because the diffusion rate depends on the rotating speed in an RDE measurement, J_d is determined by the rate at which the reactant diffuses to the surface of the electrode. When the small effect of Nafion film diffusion on the rotating electrode is neglected, the overall measured current, J, is given by the Koutecky-Levich equation (*39*, *40*):

$$\frac{1}{J} = \frac{1}{J_k} + \frac{1}{J_d} = \frac{1}{J_k} + \frac{1}{B\omega^{1/2}} \quad (1)$$

where ω is the electrode rotating rate. B is determined from the slope of the Koutecky-Levich plot based on the Levich equation below:

$$B = 0.2nF(D_{O_2})^{2/3}\upsilon^{-1/6}C_{O_2} \quad (2)$$

In Eq. 2, n represents the transferred electron number per oxygen molecules, F is the Faraday constant (F = 96,485 C mol^{-1}), D_{O_2} is the diffusion coefficient of O_2 in electrolyte, υ is the kinetic viscosity, and C_{O_2} is the bulk concentration or solubility of O_2. The constant 0.2 is adopted when the rotation speed is expressed in rpm.

Figure 1A represents the typical LSV curves of ORR tested on RDE at various rotating speeds, showing an increased J_d with increasing rotating speeds due to the enhanced oxygen diffusion to and reduction at the electrode surface. At high overpotentials, the oxygen reduction is so fast that a limiting plateau is achieved (Fig. 1A). This current plateau would be associated with the distribution of the electrocatalytic sites on the electrode surfaces (*41*). Typically, the uniform distribution of active sites leads to a fine current plateau. In contrast, the current plateau is more inclined if the distribution of active sites is less uniform and the electrocatalytic reaction is slower. n and J_k can be obtained by Koutecky-Levich plots, in which the diffusion limitation can be eliminated. Alternatively, RRDE can be used to determine the kinetics and mechanism of ORR. This technology can quantitatively evaluate the molar proportion of produced H_2O_2/HO_2^- on the ring electrode (platinum or gold, Fig. 1B). The disc and ring currents (I_D and I_R, respectively) are recorded as a function of the disc electrode potential (Fig. 1B). Taking into account that the total disc current, I_D, is the sum of the O_2 reduction currents to water, I_{H_2O}, and intermediate (H_2O_2), $I_{H_2O_2}$, and using the collection efficiency (N), we have Eq. 3:

$$I_D = I_{H_2O} + I_{H_2O_2} \quad \text{and} \quad I_{H_2O_2} = I_R/N \quad (3)$$

The H_2O_2 yield (%H_2O_2) and the electron transfer number (n) are determined by the following equations (*7*, *38*, *42*):

$$\%H_2O_2 = 200\frac{I_R/N}{I_D + I_R/N}$$
$$n = 4\frac{I_D}{I_D + I_R/N} \quad (4)$$

where N is the current collection efficiency of the ring electrode. The collection efficiency is defined as $N = -I_R/I_D$ and is usually determined by using the $[Fe(CN)_6]^{4-}/[Fe(CN)_6]^{3-}$ redox couple (*43*).

RDE and RRDE measurements are also used to evaluate the catalytic activity of electrocatalysts toward OER. As a typical example, representative OER currents of oxides collected by using a thin-film RDE are shown in Fig. 1C (*44*), which is a powerful method to determine better catalytic activity by the lower onset potential with a shaper current rise. To ensure that the observed oxidation current is from oxygen evolution, RRDE with a Pt ring can be used to detect the current for the electrochemical reduction of O_2 generated at the disc with an electrocatalyst (Fig. 1D). The measurements can also lead to insights into the reaction mechanism of OER with various electrocatalysts.

In comparison with the relatively well-established evaluation procedures for Pt-based catalysts (for example, electrochemical active surface), the electrocatalytic characterization of carbon electrocatalysts is still under development and has to be optimized. Especially, the inclined current plateau in the ORR polarization curve is commonly observed, possibly suggesting the presence of by-products (for example, H_2O_2) and/or the nonuniform distribution of active sites. Thus, the conclusion on the electrocatalytic activity of carbon-based catalysts should be reached on the basis of the proper electrode preparation. Furthermore, the performance of these electrocatalysts still needs to be further demonstrated in actual operating fuel cells or metal-air batteries.

$$\begin{aligned} &\text{Alkaline media}: O_2 + 2H_2O + 4e^- \rightarrow 4OH^- \quad \text{(Four-electron process)} \\ &O_2 + H_2O + 2e^- \rightarrow HO_2^- + OH^- \quad \text{(Two-electron process)} \\ &H_2O + HO_2^- + 2e^- \rightarrow 3OH^- \end{aligned}$$

$$\begin{aligned} &\text{Acid media}: O_2 + 4H^+ + 4e^- \rightarrow 2H_2O \quad \text{(Four-electron process)} \\ &O_2 + 2H^+ + 2e^- \rightarrow H_2O_2 \quad \text{(Two-electron process)} \\ &H_2O_2 + 2H^+ + 2e^- \rightarrow 2H_2O \end{aligned}$$

Scheme 1. The process of oxygen reduction reaction. The oxygen reduction reaction in acid and alkaline media, respectively.

HETEROATOM-DOPED CARBONS AS METAL-FREE CATALYSTS IN FUEL CELLS

A fuel cell is an electrochemical device to directly convert chemical energy into electricity by oxidizing fuels (for example, hydrogen, methanol, ethanol, and formic acid) at the anode and reducing oxygen at the cathode. Figure 2 shows the typical steady-state polarization curve of PEMFCs (*45*), which describes the relationship between the electrode potential and the current density for evaluating both ORR and fuel cell performance. The criteria to evaluate a polarization curve depend on its application (*46*). It can be seen in Fig. 2 that the fuel cell voltage is significantly deviated from the theoretical potential (also called reversible standard potential, 1.23 V) (*47*). The loss could be attributed to electrode kinetics (electron transfer overpotential), slow mass transport (diffusion overpotential), and slow chemical reactions coupled to the electron transfer (reaction overpotential). We note that the sluggish ORR is about six or more orders of magnitude slower than the hydrogen oxidation reaction in a PEMFC (*48*). Thus, ORR has a limiting

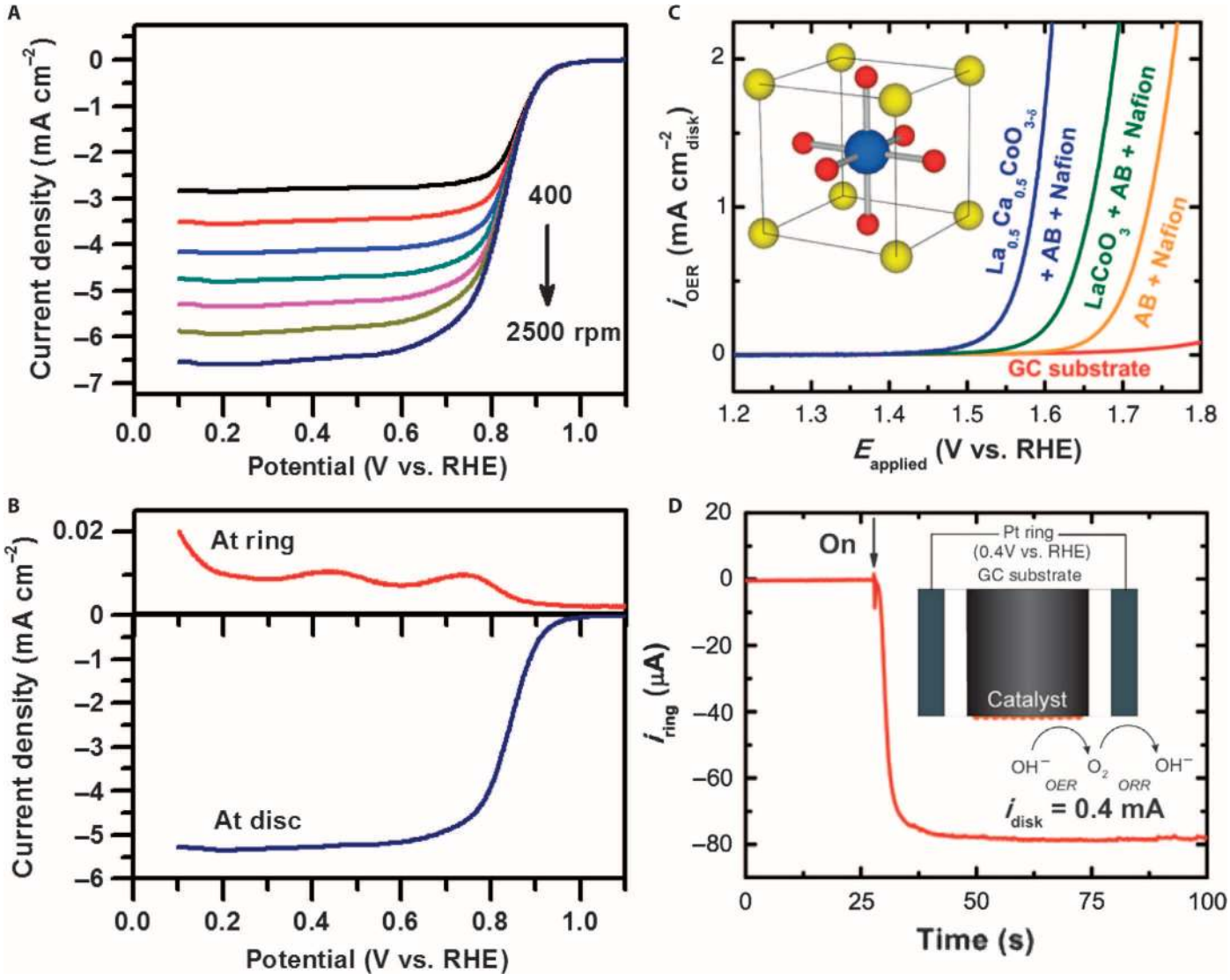

Fig. 1. Evaluation of electrocatalytic activities toward ORR and OER. (**A**) LSV curves of electrocatalysts in oxygen-saturated electrolyte with different rotating rates. (**B**) Oxygen reduction curves on the disc and ring electrodes of RRDE at 5 mV s^{-1} scan rate at 1600 rpm, respectively. (**C**) Exemplary OER currents of $La_{1-x}Ca_xCoO_3$ and $LaCoO_3$ thin films on a glassy carbon electrode (GCE) in O_2-saturated 0.1 M KOH at 10 mV s^{-1} scan rate at 1600 rpm, capacitance-corrected by taking an average of the positive and negative scans. The contributions from AB (acetylene black) and binder (Nafion) in the thin film and GCE are shown for comparison. (**D**) Evidence of O_2 generated from $Ba_{0.5}Sr_{0.5}Co_{0.8}Fe_{0.2}O_{3-d}$ (BSCF) using RRDE measurements (schematic shown as an inset). The O_2 gas generated from BSCF on a GCE disc (OER current given as i_{disc}) is reduced at the Pt ring at a constant potential of 0.4 V versus reversible hydrogen electrode (RHE). The collecting efficiency of RRED is 0.2. [From J. Suntivich, K. J. May, H. A. Gasteiger, J. B. Goodenough, Y. Shao-Horn, A perovskite oxide optimized for oxygen evolution catalysis from molecular orbital principles. *Science* **334**, 1383–1385 (2011). Reprinted with permission from AAAS.]

factor to the cell performance, which requires a platinum catalyst (see above). Because of the high cost and poor durability intrinsically associated with platinum catalysts, the development of nonprecious metal and metal-free catalysts with high ORR activities has become the major focus of fuel cell research (*15*, *49*).

To reduce or replace Pt-based electrocatalysts in fuel cells, metal porphyrins or phthalocyanines have been found to exhibit good oxygen reduction performance, but a poor stability, since the 1960s (*50*, *51*). A recent breakthrough was then achieved by mimicking the atomic configuration of metal porphyrin and phthalocyanine using individual nitrogen and Co/Fe precursors (*52*, *53*). By modifying carbon particles with polypyrrole for adsorption of cobalt ions, for example, the resultant cobalt-polypyrrole composite catalyst with C-Co-N active sites was demonstrated to combine high oxygen-reduction activity with good operation durability. More specifically, the cobalt-polypyrrole composite catalyst showed a power density of about 0.15 W cm^2 in H_2-O_2 fuel cells and did not display obvious performance degradation for more than 100 hours (*53*). Similar catalysts with C-M-N_x (typically, M = Co, Fe) have been developed by incorporating iron or cobalt into various nitrogen-rich polymer precursors, such as polypyrrole (*53*), polyaniline (*54*), phenanthroline (*55*), and 2,6-diaminopyridine (*56*), under high-temperature processes. In addition, a new class of metal-free ORR catalysts based on carbon nanomaterials doped with heteroatom(s) has recently been discovered (*7*).

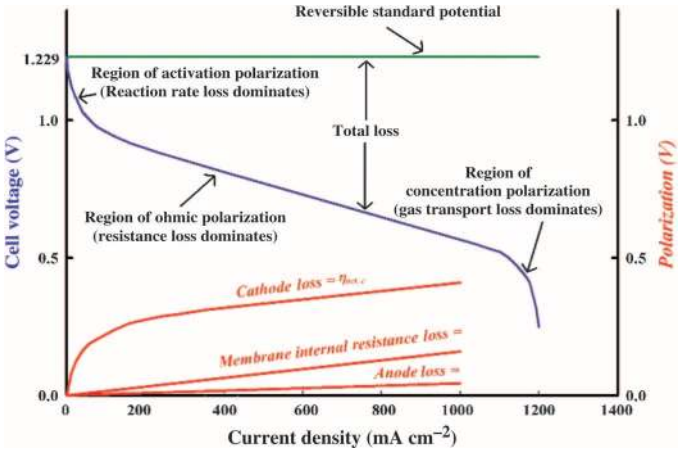

Fig. 2. Polarization curve of PEMFC. The typical polarization curve describes the relationship between cell voltage and current density used to evaluate cell performance. The various losses are shown in the same figure, indicating different overpotential sources. [From V. Ramani, H. R. Kunz, J. M. Fenton, The polymer electrolyte fuel cell. *Electrochem. Soc. Interface* **13**, 17 (2004). Reprinted with permission from the Electrochemical Society.]

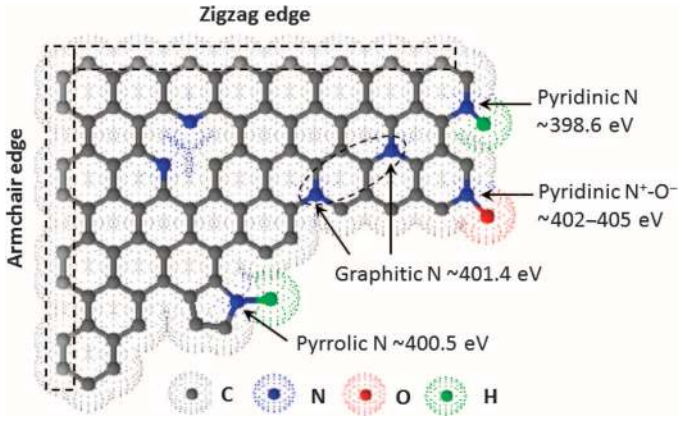

Fig. 3. Scheme illustration of nitrogen species in nitrogen-containing graphitic carbons. The commonly doped nitrogen species in graphitic carbons with the corresponding reported XPS binding energies.

Nitrogen atoms can be doped into the basal plane of a graphitic carbon (graphene) sheet in several different configurations (Fig. 3) (*57*, *58*). X-ray photoelectron spectroscopy (XPS) is a commonly used technique to examine the features of nitrogen species in N-doped carbon nanomaterials. The characteristic XPS peaks for pyridinic (N-6), pyrolic (N-5), and graphitic (N-Q) nitrogen are located at about 398.6, 400.5, and 401.4 eV (*59*, *60*), respectively, as shown in Fig. 3. These different nitrogen configurations could vary the electronic structure of neighbor carbon atoms and then affect physical and chemical properties, such as electrical conductivity and electrocatalytic activity (*61*). Previous studies have shown that the edge structure and doped-N near the edge could significantly enhance the ORR activity through the four-electron pathway (*62*, *63*). In addition, the armchair and zigzag sites located at the edges through the sp^2 hybridization are high energy sites, which could be functionalized with heteroatoms to provide strong electrochemical activities (Fig. 3). Several research groups have reported that the pyridinic N was the active site to enhance the ORR activity of the N-doped carbon materials (*9*, *64*–*71*), whereas some others suggested that more graphitic nitrogen atoms, rather than the pyridinic ones, are important for the ORR (*13*, *72*). Therefore, the exact catalytic role for each of the nitrogen forms in nanocarbon ORR catalysts is still a matter of controversy. An interconversion of the graphitic to pyridinic sites through the ring opening of a cyclic C-N bond or vice versa has been proposed to reconcile the controversy over whether the graphitic, pyridinic, or both nitrogens are active sites for ORR (*61*).

Heteroatom-doped CNTs

The location control of dopants in the heteroatom-doped carbon nanomaterials should provide us with powerful means to tailor the structure-property relationships for heteroatom-doped carbon-based metal-free catalysts. Although the accurate control of the nitrogen doping sites in carbon nanomaterials is still impossible, a few approaches, including the use of N-containing macromolecular precursors with N-rich cycles (for example, triazine and phthalocyanine derivatives) of precisely controlled locations of N atoms and hole sizes, followed by carbonization, have led to the formation of well-controlled N-doped holey graphene nanosheets (*73*, *74*). We have also used N-containing iron phthalocyanine as the precursor for the synthesis of vertically aligned NCNTs (VA-NCNTs) by chemical vapor deposition (CVD) (Fig. 4A). After removal of iron residue, if any, the VA-NCNTs thus prepared were shown to catalyze a four-electron ORR process free from CO "poisoning" with a much higher electrocatalytic activity and better durability than those of commercially available Pt/C in alkaline electrolytes (Fig. 4, B to E) (*7*). According to the experimental observations and theoretical calculations by B3LYP hybrid density functional theory (DFT), the improved catalytic performance can be contributed to the electron-accepting ability of the nitrogen atoms, which creates a net positive charge on adjacent carbon atoms in the CNT plane of VA-NCNTs (Fig. 4F). The nitrogen-induced charge delocalization could also change the chemisorption mode of O_2 from the usual end-on adsorption (Pauling model) at the nitrogen-free CNT (CCNT) surface (Fig. 4G, top) to a side-on adsorption (Yeager model) onto the NCNT electrodes (Fig. 4G, bottom). The N-doping induced charge transfer from adjacent carbon atoms could lower the ORR potential, whereas the parallel diatomic adsorption could effectively weaken the O-O bonding, facilitating ORR at the VA-NCNT electrodes. Uncovering this ORR mechanism in the NCNT electrodes is significant because the same principle has been applied to the development of various other metal-free efficient ORR catalysts for fuel cells and other applications (*17*, *35*).

To examine the chemical nature of active sites and optimize the content of nitrogen in carbon lattices for ORR, many groups, including our own ones, have synthesized NCNTs with different nitrogen contents using different precursors (*17*, *75*–*78*). For instance, NCNT/nanoparticle composites were obtained from iron acetate as an iron precursor and from cyanamide as a nitrogen and CNT precursor for ORR electrocatalysts (*79*). NCNTs with relatively high nitrogen contents have also been prepared by increasing the precursor ratio (pyridine to ethanol) for CVD (*58*). Such NCNTs exhibited a positive correlation between nitrogen content and electrocatalytic activity toward ORR. The nitrogen contents in NCNT arrays have also been adjusted by changing the pyrolysis temperature. The NCNTs with a high content of pyridinic-type nitrogen showed excellent activity toward ORR and much better activity in alkaline medium than that in an acidic medium (*80*). The influence of nitrogen concentration in the NCNTs on the electronic, structural, and electrochemical properties has been examined, showing an increase in the bulk electrical conductivity and the density of states at the Fermi level with the increased nitrogen

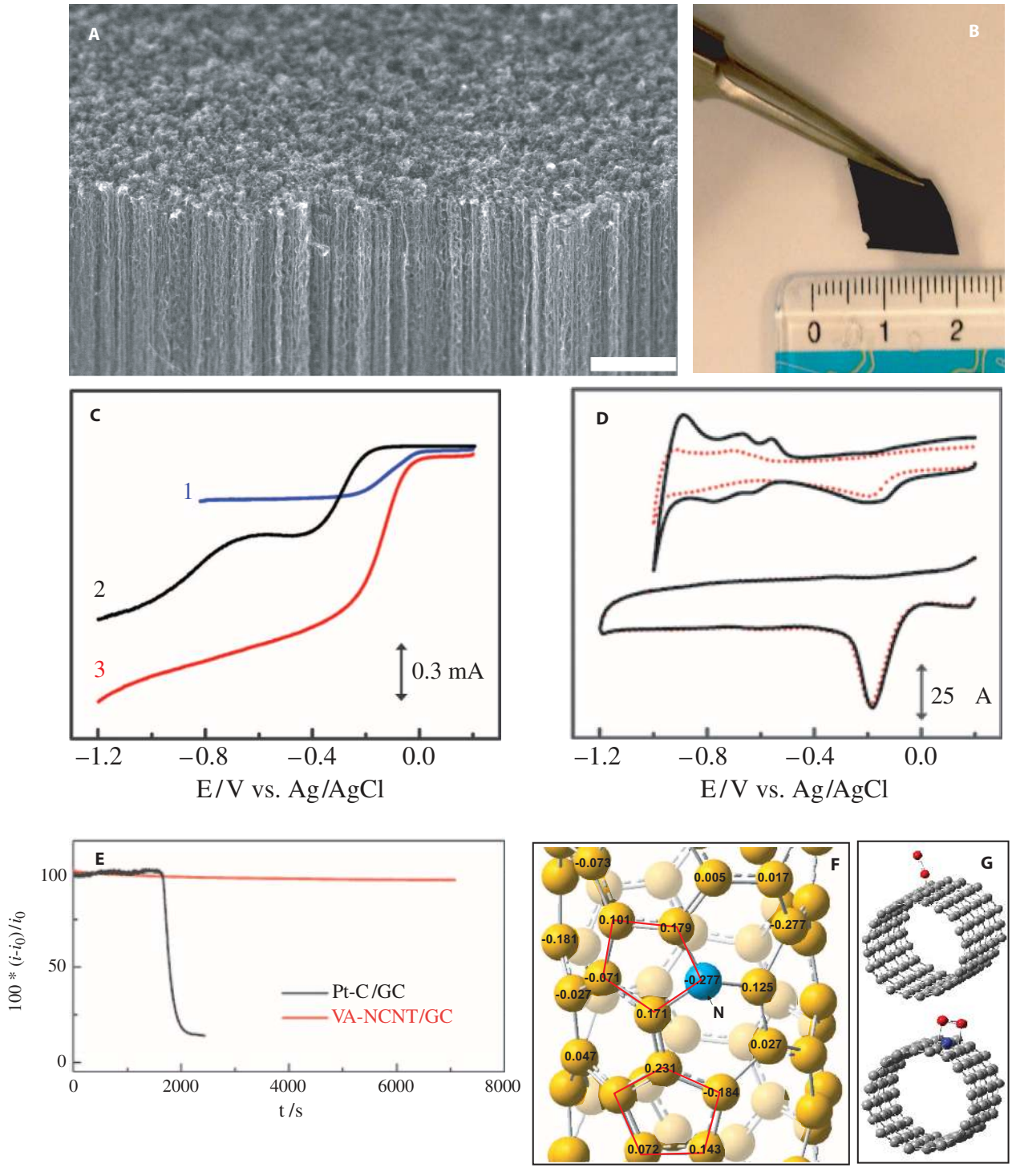

Fig. 4. Morphology characterization and catalytic performance of VA-NCNTs. (**A**) Scanning electron microscopy image of the as-synthesized VA-NCNTs on a quartz substrate. Scale bar, 2 μm. (**B**) Digital photograph of the VA-NCNT array after having been transferred onto a polystyrene (PS) and nonaligned CNT conductive composite film. (**C**) RDE voltammograms for oxygen reduction in air-saturated 0.1 M KOH at the Pt/C (curve 1), VA-CCNT (curve 2), and VA-NCNT (curve 3) electrodes. (**D**) Cyclic voltammograms for the ORR at the Pt/C (top) and VA-NCNT (bottom) electrodes before (solid curves) and after (dotted curves) a continuous potentiodynamic sweep for about 100,000 cycles in air-saturated 0.1 M KOH at room temperature (25 ± 1°C). Scan rate: 100 mV s^{-1}. (**E**) The CO poisoning effect on the *i-t* chronoamperometric response for the Pt/C (black curve) and VA-NCNT (red line) electrodes. CO gas (55 ml/min) was first added into the 550 ml/min O_2 flow, and then the mixture gas of ~9% CO (v/v) was introduced into the electrochemical cell at about 1700s. (**F**) Calculated charge density distribution for the NCNTs. (**G**) Schematic representations of possible adsorption modes of an oxygen molecule at the CCNTs (top) and NCNTs (bottom). [From K. Gong, F. Du, Z. Xia, M. Durstock, L. Dai, Nitrogen-doped carbon nanotube arrays with high electrocatalytic activity for oxygen reduction. *Science* **323**, 760–764 (2009). Reprinted with permission from AAAS.]

doping in CNTs (*71*).This could also result in chemically active, localized areas of higher electron density to promote the electrocatalysis of ORR. Theoretical simulations indicated that the presence of nitrogen could reduce the barrier to ORR at neighbor carbon atoms (*81*).

Because the CVD process for producing the VA-NCNTs involves metal catalysts (for example, Fe), considerable care has been taken during the electrode preparation to completely remove the catalyst residue. However, there are still some concerns on the possible effects of metal contaminates on the observed superb ORR performance (*82*–*84*) unless N-doped carbon materials with excellent ORR electrocatalytic activities can be produced by a metal-free preparation procedure. In this context, NCNTs with a high nitrogen doping level (~20 atomic %) have recently been synthesized directly by using melamine as a C/N precursor in the absence of metal catalyst (*77*), displaying excellent ORR catalytic activity comparable to that of Pt/C catalysts with outstanding stability, fuel selectivity, and resistance to CO poisoning. Similarly, many other heteroatom-doped carbon nanomaterials generated from metal-free preparation procedures also showed outstanding ORR activities in both alkaline and acid electrolytes (*13*, *64*, *85*–*88*). Therefore, the observed ORR activities in these cases are exclusively attributed to intrinsic nonmetal active sites in N-doped carbons.

Subsequent studies extended to the other heteroatoms with different electronegativities (x) from that of carbon (x = 2.5), such as boron (x = 2.0) and phosphorus (x = 2.1), for enhancing the ORR activity. For instance, Yang *et al.* (*18*) have demonstrated that boron with a lower electronegativity than carbon could dope CNTs into metal-free ORR catalysts with positively shifted potentials and enhanced reduction current, as well as good stability and high resistance toward methanol crossover and CO poisoning. The experimental and theoretical results suggest that the doping-induced charge redistribution, regardless of whether the dopants have a higher (as N) or lower (as B) electronegativity than that of carbon, could create charged sites (C^+ or B^+) that are favorable for O_2 adsorption and subsequent reduction process (*17*). We have successfully prepared vertically aligned CNTs containing both nitrogen and boron heteroatoms (VA-BCN) and found that the resultant VA-BCN nanotubes exhibited a higher electrocatalytic activity for ORR in alkaline medium than VA-CNTs doped with either boron or nitrogen only (*89*). Thus, the dual-doped CNTs with heteroatoms, one with higher and one with lower negativity than that of carbon, showed a synergetic effect arising from the co-doping (*20*). Theoretical calculations revealed that co-doped CNTs with separated B-C and N-C are capable of turning the inert CNTs into efficient ORR catalysts, whereas the bonded boron and nitrogen (B-N-C) cannot because charge neutralization between the bonded boron and nitrogen leads to unfavorable chemisorption of O_2 on the co-doped CNTs (*90*). Experimentally, the observed co-doping–induced synergetic effect has been applied to CNTs co-doped with other heteroatoms, including phosphorus (P), sulfur (S), and nitrogen (N), for high-performance electrocatalysis of ORR (*21*, *90*–*92*), and opens up novel avenues for designing various efficient metal-free ORR catalysts through co-doping carbon nanomaterials with more than one heteroatoms of different electronegativities.

In addition to the ORR activities arising from the heteroatom-doping–induced intramolecular charge redistribution discussed above, poly(diallyldimethylammonium chloride)-adsorbed undoped CNTs were also demonstrated to act as metal-free catalysts for ORR through the intermolecular charge transfer from the all-carbon CNTs to the adsorbed polyelectrolyte (*23*). More recently, phosphorus-encapsulated single-walled carbon nanotubes (SWNTs) were also demonstrated to exhibit improved ORR activity, though relatively inferior to the commercial Pt/C electrode, due to the good electron-accepting properties of the filled phosphorus clusters that create a large number of positively charged sites on the carbon plane (*93*). These results indicate the important role of intermolecular charge transfer to ORR for carbon nanomaterials.

Heteroatom-doped graphene

Graphene, a 2D single-atom-thick layer of sp^2 hybridized carbons tightly bonded in a hexagonal lattice, is the basic building block for all other graphitic carbons, including CNTs. Having many similarities to CNTs in structure and property, such as high aspect ratio (the ratio of lateral size to thickness), large surface area, rich electronic states, and good mechanical properties, graphene is an attractive candidate for potential uses in many areas where the CNTs have been exploited. In comparison with CNTs, the graphene sheets with a 2D planar geometry will further facilitate electron transport, and hence are efficient electrode materials for potential uses as metal-free ORR catalysts (*35*, *94*, *95*).

Soon after the discovery of ORR activity of the VA-NCNTs (*7*), Qu *et al.* (*9*) further demonstrated that N-doped graphene (NG) films produced by CVD in the presence of ammonia had a superb ORR performance in alkaline medium that was comparable to that of VA-NCNTs with the same nitrogen content. Like NCNTs, the electronic and chemical properties of graphene can also be modulated by chemical doping with heteroatoms (*96*). Unlike NCNTs, graphene materials and their N-doped derivatives with different sizes, qualities, and prices for various specific applications can be produced by CVD and arc discharge of graphite electrodes as well as various large-scale preparation methods, such as liquid-phase exfoliation and molecular assembling (Fig. 5) (*97*). For instance, a novel method for one-pot direct synthesis of NG through the reaction of tetrachloromethane with

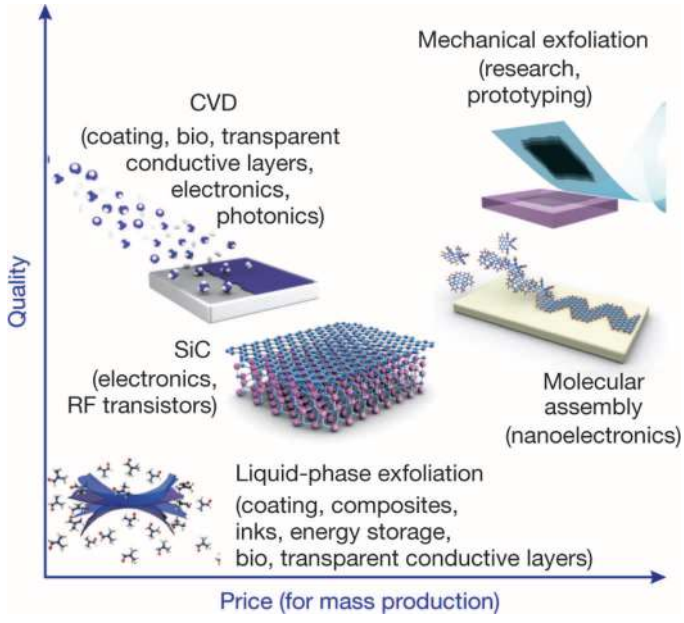

Fig. 5. Scheme illustration of methods for mass production of graphene. The various methods for graphene production allowing a wide choice in terms of size, quality, and price for specific applications. [From K. S. Novoselov, V. I. Fal'ko, L. Colombo, P. R. Gellert, M. G. Schwab, K. Kim, A roadmap for graphene. *Nature* **490**, 192–200 (2012). Reprinted with permission from the Nature Publishing Group.]

lithium nitride under mild conditions has been reported (*98*), which led to a nitrogen content in the range of 4.5 to 16.4% and an enhanced catalytic ORR activity with respect to pure graphene and commercial carbon black XC-72. Multilayered NG films with a uniform structure and a nitrogen content of 12.5% have also been synthesized from a detonation reaction between cyanuric chloride and trinitrophenol (*99*). In a phosphate buffer solution, the resultant NG acted as a metal-free electrode with an excellent electrocatalytic activity and long-term operation stability for ORR through combined two- and four-electron pathways.

Graphitic carbon nitride, g-C_3N_4, a carbonaceous material that has a planar phase analogous to graphite, has also been extensively investigated for metal-free electrocatalysis of ORR (*100*, *101*). g-C_3N_4 can be readily obtained through the pyrolysis of cyanamide (*102*), melamine (*103*), ethylenediamine/carbon tetrachloride (*104*), or *s*-triazine derivatives (*105*) through condensation. Lyth *et al.* (*106*) investigated the ORR activity of carbon nitride in oxygen-saturated sulfuric acid solution and found a much higher onset potential of 0.69 V (versus NHE) than that (0.45 V) for a carbon black reference electrode. A relatively low current density for the carbon nitride electrode (0.72 versus 0.91 mA cm^{-2} for the carbon black electrode) was observed, which could be attributed to its low surface area (5 m^2 g^{-1}) and poor electric conductivity. In the same study, a significant improvement in both current density (2.21 mA cm^{-2}) and onset potential (up to 0.76 V) was achieved by blending the carbon nitride with a high surface area carbon black support (50 wt %). To prepare carbon nitride materials with enhanced electrical conductivity and surface accessibility, several innovative approaches have been devised by incorporating g-C_3N_4 into mesoporous carbon with a large surface area (*16*), immobilizing g-C_3N_4 onto chemically converted graphene (CCG) sheets to form a composite (G-g-C_3N_4) through polymerization of melamine molecules adsorbed on CCG sheets at a high temperature of 823 K (*107*), and preparing the macroporous g-C_3N_4/C with 3D ordered interconnected structures using silica microspheres as hard templates (*86*). These methods led to g-C_3N_4 composites with an enhanced electron transfer efficiency, ORR catalytic activity, fuel crossover resistance, and long-term durability, comparable to or, even better, than that of the commercial Pt/C in alkaline medium. On the other hand, Yang *et al.* (*108*) fabricated g-C_3N_4 nanosheets with interdispersed graphene layers to show a high nitrogen content, high surface area, large aspect ratio, and enhanced electrical conductivity attractive for electrocatalysis.

Alternatively, the solution oxidation of graphite with strong oxidizing reagents (for example, HNO_3, $KMnO_4$, and/or H_2SO_4) to produce solution-processable graphene oxide (GO) sheets with reactive carboxylic acid groups at the edge and epoxy and hydroxyl groups on its basal plane is one of the most popular methods for mass production of soluble graphene materials (*109*, *110*). Subsequent reduction of GO sheets using a reducing regent or thermal treatment led to electrically conductive reduced graphene oxide (RGO) sheets on a large scale. N-doped RGO (NRGO) can be prepared by posttreatments of GO (or RGO) with various nitrogen-containing species, including ammonia (*111*), melamine (*112*), polyaniline (*113*), pyrrole (*114*), urea (*115*), and ionic liquid (*114*). These approaches could avoid the contamination of metal catalysts, and thus, the intrinsic catalytic performance of metal-free doped graphene can be examined. Using melamine as the nitrogen precursor, Sheng *et al.* (*112*) reported that the atomic percentage of nitrogen in NRGO samples could be adjusted up to 10.1%, mainly containing pyridine-like nitrogen atoms. Pyrolysis of well-mixed GO and urea in an inert environment has also resulted in the formation of NRGO with a high percentage of graphitic nitrogen, in which GO was thermally reduced and N atoms were doped into the graphitic lattice (*115*). The resultant NRGO exhibited a high catalytic activity toward the ORR through a four-electron pathway with superior stability and anti-crossover property to Pt/C catalysts. In addition, Lai and co-workers (*113*) have demonstrated that the bonding state of the N atom had a significant effect on the selectivity and catalytic activity for ORR. Specifically, these authors found that graphitic and pyridinic N centers were preferentially formed by annealing GO with ammonia, whereas annealing of polyaniline/RGO and polypyrrole/RGO tended to generate pyridinic and pyrrolic N moieties. It has been revealed that pyridinic N can contribute one *p*-electron to the aromatic system and has a lone electron pair in the plane of carbon matrix, which can increase the electron-donor property of the catalyst. Thus, it would weaken the O-O bond through the bonding between oxygen and nitrogen and/or the adjacent carbon atom to facilitate the reduction of O_2. However, the total N content in the NRGO catalyst played a much less important role in the ORR process in this particular case.

In addition to N-doping, graphene materials doped with other heteroatoms, such as S (*10*), P (*116*), B (*117*), and halogen (*21*), have also been studied. Among them, sulfur has a similar electronegativity to that of carbon, and hence no doping-induced charge transfer. Nevertheless, graphene materials doped with sulfur also exhibit better catalytic activity than do the commercial Pt/C in alkaline media (*10*), presumably due to the doping-induced spin redistribution effect (*12*). Doping graphite layers with P, an element of the same number of valence electrons and similar chemical properties as N, by pyrolysis of toluene and triphenylphosphine (TPP) also showed high electrocatalytic activity toward the ORR, long-term stability, and excellent tolerance to the methanol crossover effect in alkaline medium (*116*). These results not only shed light on the metal-free ORR mechanism for the doped carbon nanomaterials but also open new ways for scalable fabrication of other low-cost, metal-free electrocatalysts.

Recent efforts have led to solution-processable edge-functionalized graphene (EFG) sheets. Through a simple one-pot reaction, for example, Jeon and co-workers (*118*) have prepared edge-functionalized graphene nanoplatelets (EFGnPs) with aminobenzoyl moiety, which could be used as the in situ feedstock for "C-welding" and "N-doping" to produce high-quality NG films without introducing any oxygen-containing surface groups on the graphene basal plane. By solution casting the NG on a GC electrode and subsequent heat treatment, these authors demonstrated comparable ORR performance to the NG prepared by CVD. On the other hand, Jeon and co-workers (*119*) have also developed a low-cost and scalable ball milling method to produce high-quality, edge-functionalized NG films. By ball milling graphite with dry ice in a planetary ball-mill machine, Jeon and co-workers (*119*) initially produced edge-selectively carboxylated graphite (ECG), which is highly dispersable in many solvents to self-exfoliate into single- or few-layer graphene sheets. By replacing dry ice with N_2 gas, the same authors have developed a simple approach to direct fixation of N_2 into graphene nanoplatelets (GnPs) to form five- and six-membered aromatic rings at the broken edges (*120*), leading to solution-processable edge-nitrogenated graphene nanoplatelets (NGnPs) with superb electrocatalytic performance. As shown in Fig. 6, ball milling graphite in the presence of reactants other than dry ice or N_2 (for example, halogen) is an efficient approach to scalable production of EFGnPs with various edge-functional groups (Fig. 6A) (*21*, *119*). For instance, GnPs functionalized with hydrogen (HGnP), carboxylic acid (CGnP), sulfonic acid (SGnP), and mixed carboxylic acid/sulfonic acid (CSGnP) have been synthesized in the presence of hydrogen, carbon dioxide, sulfur trioxide, or carbon dioxide/sulfur trioxide mixture (*21*, *119*). One of the salient features of

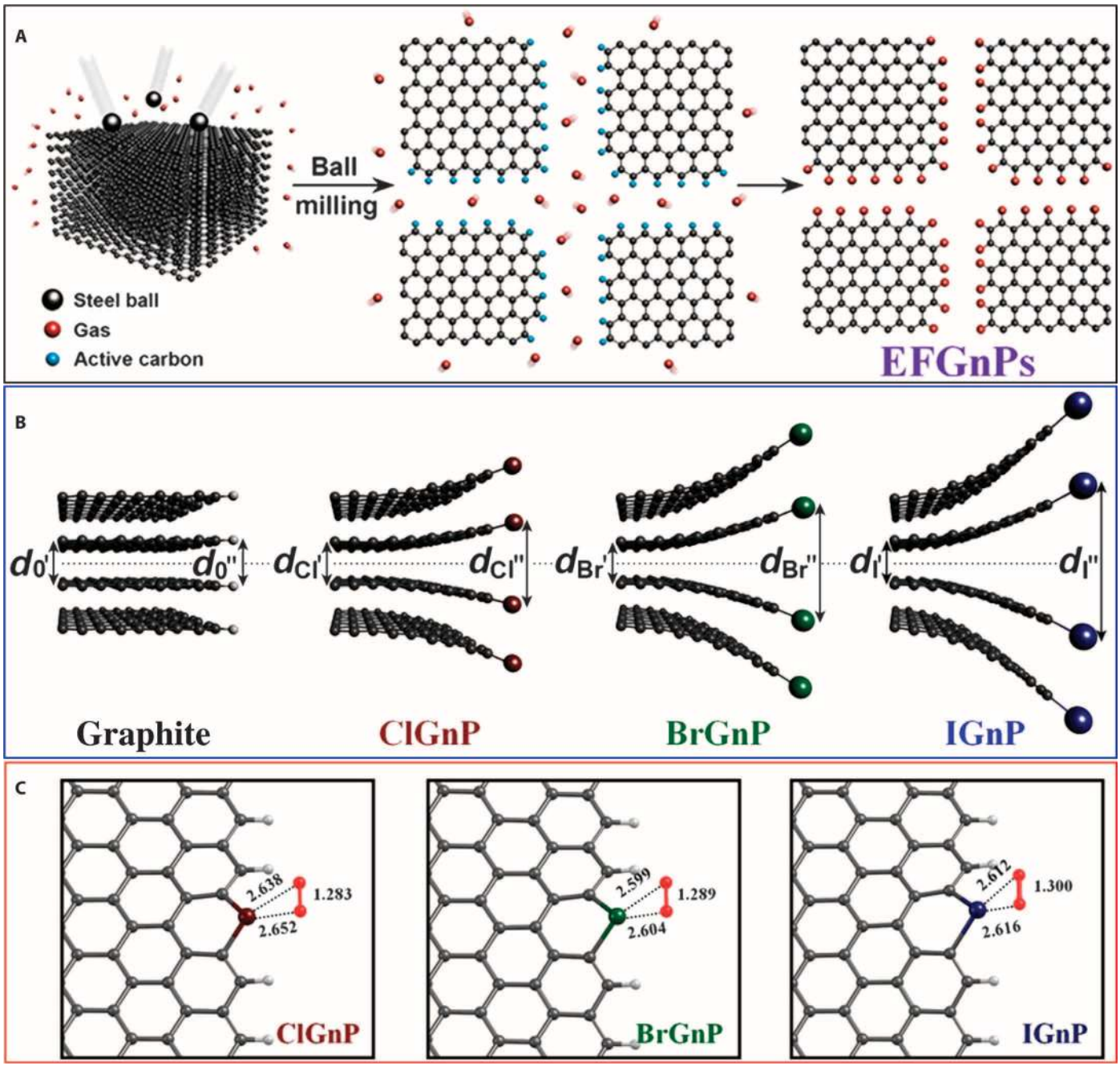

Fig. 6. Schematic illustration of the preparation of EFGnPs through the ball-milling method for ORR. (**A**) Schematic representation of the mechanochemical reaction between in situ generated active carbon species and reactant gases in a sealed ball-mill crusher. The cracking of graphite by ball milling in the presence of corresponding gases and subsequent exposure to air moisture resulted in the formation of EFGnPs. The red balls stand for reactant gases such as hydrogen, carbon dioxide, sulfur trioxide, and air moisture (oxygen and moisture). [Derived from (*119*), Copyright 2012 National Academy of Sciences.] (**B**) A schematic representation for the edge expansions of XGnPs caused by the edge halogens: ClGnP, BrGnP, and IGnP. (**C**) The optimized O_2 adsorption geometries onto XGnPs, in which halogen covalently linked to two sp^2 carbons. In (C), the O-O bond length and the shortest C-O bond are shown in angstrom. [From I.-Y. Jeon, H.-J. Choi, M. Choi, J.-M. Seo, S.-M. Jung, M.-J. Kim, S. Zhang, L. Zhang, Z. Xia, L. Dai, N. Park, J.-B. Baek, Facile, scalable synthesis of edge-halogenated graphene nanoplatelets as efficient metal-free eletrocatalysts for oxygen reduction reaction. *Sci. Rep.* **3**, 1810 (2013). Reprinted with permission from the Nature Publishing Group.]

EFGnPs is that the reaction medium does not intercalate into graphite but selectively functionalizes the sp^2 C-H defects at the edges of graphite, leading to minimal carbon basal plane damage, and hence the formation of highly conductive electrodes. Electrochemical measurements indicated that the ORR activity of EFGnP electrodes follows the order of SGnP > CSGnP > CGnP > HGnP > pristine graphite. Among them, the sulfur-containing SGnP and CSGnP have superior ORR performance to the Pt/C electrocatalysts. Oxidation of SGnP into

SOGnP further improved the ORR catalytic activity (*12*). Theoretical calculations showed that the electronic spin density, in addition to generally considered charge density, played a key role in the high ORR activity of SGnP and SOGnP. Furthermore, both SGnP and SOGnP demonstrated a better fuel selectivity with a longer-term stability than those of the pristine graphite and commercial Pt/C electrocatalysts.

It is worth mentioning that the dry ball milling method is quite general. By ball milling graphite with Cl_2, Br_2, and I_2, a series of edge-selectively halogenated GnPs (XGnPs, X = Cl, Br, I) have been prepared (Fig. 6B) (*21*). Although the electron negativities of halogen atoms are in the order of Cl (x = 3.16) > Br (x = 2.96) > I (x = 2.66), the experimentally observed electrocatalytic activities for ORR are in the order of IGnP > BrGnP > ClGnP. Compared to the pristine graphite and Pt/C, IGnP exhibited much better electrocatalytic performances with an excellent long-term durability and tolerance to methanol crossover/CO poisoning effects. Considering the difference in the electronegativity between halogens (Cl x = 3.16, Br x = 2.96, and I x = 2.66) and carbon (x = 2.55), the reversed order of ORR activities, ClGnP << BrGnP < IGnP, seems contradictory to the doping-induced charge transfer effect (*7*). In comparison to Cl, however, Br and I can form partially ionized bonds of -Br^+- and -I^+- to further enhance the charge transfer because of their relatively larger atomic sizes. The larger atomic size leads to more loosely bound valence electrons for easy charge polarization in the BrGnP and IGnP electrodes. According to DFT calculations, halogenated edges, in which halogen atoms substitute for the C sites in the zigzag edges, show desirable binding affinity with O_2 molecules (Fig. 6C). The efficiency of the charge transfer between the halogen and adsorbed O_2 follows the atomic size in the order of Cl < Br < I. The charge transfer–induced weakening of the O-O bond strength is most prominent for the case of IGnP, leading to the best catalytic activity. These new insights on the ORR of the edge-functionalized GnPs could provide practical approaches to designing high-performance metal-free ORR electrocatalysts through low-cost and scalable ball milling techniques, which have many advantages over the commonly used solution synthetic method (*118*).

Similarly to co-doped CNTs, co-doping graphene with two heteroatoms, one with higher (for example, N, x = 3.04) and another with lower (for example, B, x = 2.04) electronegativity than that of C (x = 2.55), can create a unique electronic structure, leading to synergistic effects with a higher electrocatalytic activity than singly doped counterparts. In this context, we have successfully developed a facile low-cost approach to mass production of co-doped graphene with tunable N-/B-doping levels simply by thermally annealing RGO in the presence of boric acid in ammonia atmosphere (*20*). The first-principles calculations revealed a doping-level–dependent energy bandgap, spin density, and charge density. The substitution of C with B and N led to a smaller energy gap. However, overdoping of B and N showed a detrimental effect on the conjugation length, which is accompanied by a drastic increase in the energy gap and a reduced conductivity, significantly affecting its electron transfer and catalytic capability. In agreement with the theoretical results, BCN graphene with a modest N- and B-doping level was demonstrated to have the best ORR electrocatalytic activity, fuel selectivity, and long-term durability, along with an excellent thermal stability and porosity. Subsequently, a two-step method was developed for incorporating N and B sequentially into selected sites of the graphene domain to further enhance the electrocatalytic activity toward ORR (*19*).

The co-doping–induced synergistic effect has also been observed when S and N were simultaneously incorporated into graphene to form dual-doped graphene (*86*). S and N co-doped graphene (N-S-G) materials with large mesopores favorable for mass transfer (*86*) were found to exhibit a good electrocatalytic activity, long durability, and high selectivity for ORRs, comparable to that of commercial Pt/C and significantly better than that of graphene catalysts doped solely with S atoms (S-G) or with N atoms (N-G). Although the similar electronegativities between S (x = 2.58) and C atoms (x = 2.55) resulted in a negligible charge transfer between S and C, the DFT calculations indicated that the dual doping of S and N induced asymmetrical spin and charge density in the N-S-G models with different relative positions of the S and N atoms, leading to the excellent ORR performance observed for the dual-doped N-S-G catalysts.

Heteroatom-doped 3D carbon nanostructures

Carbon nanomaterials with unique 3D ordered porous nanostructures of a controllable pore diameter and configuration, good mechanical and chemical stability, high graphitization degree, and high surface area have attracted a great deal of interest for a wide range of applications, including gas adsorbents, catalyst supports, and electrodes in supercapacitors (*29*, *121*–*126*). Heteroatom-doped 3D porous carbons have been synthesized from various dopant-containing precursors by using ordered mesoporous silica as a hard template. For example, Liu *et al.* (*13*) have used ordered mesoporous silica SBA-15 as a template and a nitrogen-containing aromatic dyestuff, *N*,*N*′-bis(2,6-diisopropyphenyl)-3,4,9,10-perylenetetracarboxylic diimide (PDI), as the carbon precursor to synthesize 3D N-doped mesoporous carbon with a high ORR electrocatalytic activity, excellent long-term stability, and good resistance to crossover effects. Owing to the metal-free preparation procedure, the observed electrocatalytic activity can be exclusively attributed to the incorporation of nitrogen in the mesoporous carbon. By using SBA-15 mesoporous silica with different channel lengths as templates, phosphorus-doped ordered mesoporous carbons (POMCs) have also been synthesized from triphenylphosphine and phenol as phosphorus and carbon sources, respectively (*127*). The resultant POMCs of a low P doping level (less than 1.5 atomic %) acted as a metal-free electrode for ORR through a four-electron pathway in alkaline medium with an excellent electrocatalytic activity, along with an enhanced stability and alcohol tolerance with respect to platinum. It was found that POMCs with a shorter channel length (~0.7 μm) exhibited better electrocatalytic performance. In addition, N-doped 3D carbon nanocages, with a large specific surface area up to 1393 $m^2\ g^{-1}$ and superior ORR stability to the commercial Pt/C electrocatalyst in alkaline medium, were prepared through in situ synthesis from pyridine precursor within an MgO template (*11*).

Through in situ polymerization of polyaniline within the pores of the SBA-15 template, N and O co-doped mesoporous carbons have also been synthesized recently (*128*). The resultant 3D porous carbons showed good activities toward ORR because of the synergistic effect of the O and N co-doping. Similarly, the SBA-15 template was used to prepare S and N co-doped 3D carbon foams (S-N-CF) with controllable morphologies from sucrose and thiourea (*129*). Compared to a commercial Pt/C catalyst, the resultant S-N-CF exhibited a better catalytic activity, longer-term stability, and higher methanol tolerance, attributable to multiple synergistic effects intrinsically associated with the co-doping and unique 3D architecture, including (i) numerous ORR catalytic sites from the high S and N heteroatom loadings, (ii) good reactant transports through the 3D pore structures, and (iii) efficient electron transfer along the 3D continuous carbon networks. In addition, N and S co-doped 3D

carbon aerogels with distinct morphologies and controllable S-doping levels have been synthesized through hydrothermal carbonization of *S*-(2-thienyl)-L-cysteine (TC) and 2-thienyl carboxaldehyde (TCA), followed by thermal annealing to further modulate the conductivity and heteroatom binding states (*130*). The N and S co-doped carbon aerogels showed an improved electrocatalytic activity with respect to the solely N-doped carbon aerogel, in both basic and acidic media. These results indicate that nanostructured carbon electrodes with 3D architectures of a large specific surface area can facilitate ion diffusion/charge transfer and are highly desirable for electrocatalysis.

Heteroatom-doped carbon electrocatalysts for ORR in acid media

As can be seen from the above discussions, most recent studies on the metal-free electrocatalysts based on heteroatom-doped carbon nanostructures have focused on the ORR reaction in alkaline electrolytes. However, fuel cells that operate with acidic electrolytes, particularly PEMFCs (*47*), could have a more significant economic impact. Although many doped carbons have exhibited robust electrocatalytic activity toward ORR in alkaline electrolytes, their ORR activities are still inferior to platinum catalysts under acidic conditions, probably because of the relatively few catalytic sites formed on the carbons (*65*). Therefore, many recent efforts have been devoted to modulating various physicochemical characteristics of heteroatom-doped carbon nanomaterials, such as the carbon edge sites, doping amount, type of doping, surface area, and degree of sp^2 bonding in the carbon matrix, to enhance their catalytic activities in acidic solutions. In this context, we have developed a simple plasma etching technology to effectively generate SiO_2 nanoparticles as nonmetal catalysts for efficient growth of N-doped SWNTs by pyrolysis of CH_4 under NH_3 at 900°C (*64*). Compared with undoped CNTs, the newly produced metal-free NCNTs showed relatively good electrocatalytic activity and long-term stability toward ORR in an acidic medium. In addition, a metal-free ordered mesoporous carbon nitride (OMCN) has been prepared for ORR in an acidic medium to show significantly enhanced electrocatalytic activity compared to bulk carbon nitride and ordered mesoporous carbon in terms of both the current density and onset potential (*131*). A high surface area and an increased density of catalytically active nitrogen groups in the OMCN could concomitantly contribute to its enhanced performance. Furthermore, the OMCN also exhibited a superior durability and methanol tolerance to a Pt/C catalyst, suggesting its potential utilization as an electrocatalyst for PEMFCs.

To increase the catalytic activity of N-doped carbons in acidic media, co-doping with additional dopants of B and/or P was also investigated (*92*). It was noted that co-doping with B reinforced the sp^2 structure of graphite and increased the portion of pyridinic N sites in the carbon lattice, whereas P co-doping enhanced the charge delocalization of the carbon atoms and produced carbon structures with many edge sites. These co-doping–induced physical and structural alternations of the N-doped carbons are responsible for the enhanced ORR activity. Compared with N-doped carbon, B, N co-doped and P, N co-doped carbons showed 1.2 and 2.1 times higher ORR activities, respectively, in acidic media. The ternary-doped carbon (B, P, N–doped carbon) exhibited the highest ORR catalytic activity, 2.3 times higher than that of its N-doped counterpart (*92*). These results imply that the binary or ternary doping of B and P with N into carbon nanomaterials significantly enhanced the ORR performance, presumably owing to the improved charge delocalization of the carbon atoms and increased number of edge sites.

To increase the number of edge (defect) sides, a new type of ORR electrocatalysts based on few-walled (two to three walls) CNTs and graphene hybrids has been developed through a unique oxidation condition, in which abundant defects were introduced through partial unzipping of the outer nanotube walls to form large amounts of defect-rich nanoscale graphene sheets intimately attached to the intact inner walls of the CNTs (*130*). The edge- and defect-rich graphene sheets facilitated the formation of catalytic sites on annealing in NH_3 to show a high ORR activity and superb stability for ORR in acidic solutions. In this particular case, however, it is difficult to eliminate the effect of iron impurities originated from catalyst residues on nanotube growth because iron atoms could be found next to nitrogen atoms along the edges of the defective graphene sheets attached to the intact inner walls of few-walled nanotubes.

More recently, we have developed a new class of carbon-based metal-free ORR catalysts that worked well in acid PEMFCs (*25*). By mixing NG with acid-oxidized CNTs and carbon black particles in solution, followed by freeze-drying, we obtained 3D porous carbon foams (N-G-CNT), in which N-graphene provided enormous surface area to speed ORR, nanotubes enhanced conductivity, and carbon black separated the graphene sheets for free flow of the electrolyte and oxygen, which altogether greatly increased the ORR performance and efficiency of the N-G-CNT electrode. The cell performance of PEMFC at the N-G-CNT loading of 0.15, 0.5, or 2 mg cm^{-2} plus 2 mg cm^{-2} carbon black [Ketjenblack (KB)] is given in Fig. 7A, which shows a dramatic activity suppression for the cathode with high catalyst loadings (2 mg cm^{-2}), as shown by the retardation in the activity increase with increasing catalyst loading (Fig. 7A). Figure 7B shows a current of 30 A g^{-1} at 0.8 V, a limiting current of 2000 A g^{-1} at 0.1 V, and a peak power density of 300 W g^{-1} for the N-G-CNT with carbon black (N-G-CNT/KB/Nafion = 0.5:2:2.5 mg cm^{-2}), which are comparable to high-performance Fe(Co)/N/C catalysts (*25*). In comparison with the Fe/N/C nonprecious metal catalyst, N-G-CNT + KB (at both low and high loadings) showed a comparable capacity with a much better durability in PEMFCs operating at a constant voltage of 0.5 V with pure H_2/O_2 as fuel gas (Fig. 7C). Because carbon is more anticorrosive to acids than most transition metals, no significant acidic corrosion was observed for the carbon electrode. As can be seen in Fig. 7C, N-G-CNT + KB exhibited an excellent stability with a relatively small current decay (~20% decay over 100 hours). In contrast, the Fe/N/C catalyst showed an initial sharp current decay with a total of about 75% decay over 100 hours at both the high (2 mg cm^{-2}) and low loadings (0.5 mg cm^{-2}) (*25*). This work indicates that N-doped carbon nanomaterials are durable catalysts for ORR in acidic fuel cells (for example, PEMFCs), and opens possibilities for clean energy generation from affordable and durable PEMFCs based on low-cost, metal-free, carbon-based ORR catalysts.

HETEROATOM-DOPED CARBONS FOR METAL-AIR BATTERIES

Metal-air battery is an electrochemical energy device in which a porous electrode allows the specific metal to react directly with O_2 from the air for electricity generation and storage. Because of the large theoretical specific capacity of metal anode materials (for example, 3842 mAh g^{-1} for Li, 3816 mAh g^{-1} for Si, 2965 mAh g^{-1} for Al, 2204 mAh g^{-1} for Mg, and 815 mAh g^{-1} for Zn), metal-air batteries are attracting considerable attention nowadays (*132*). Although different metals and electrolytes are

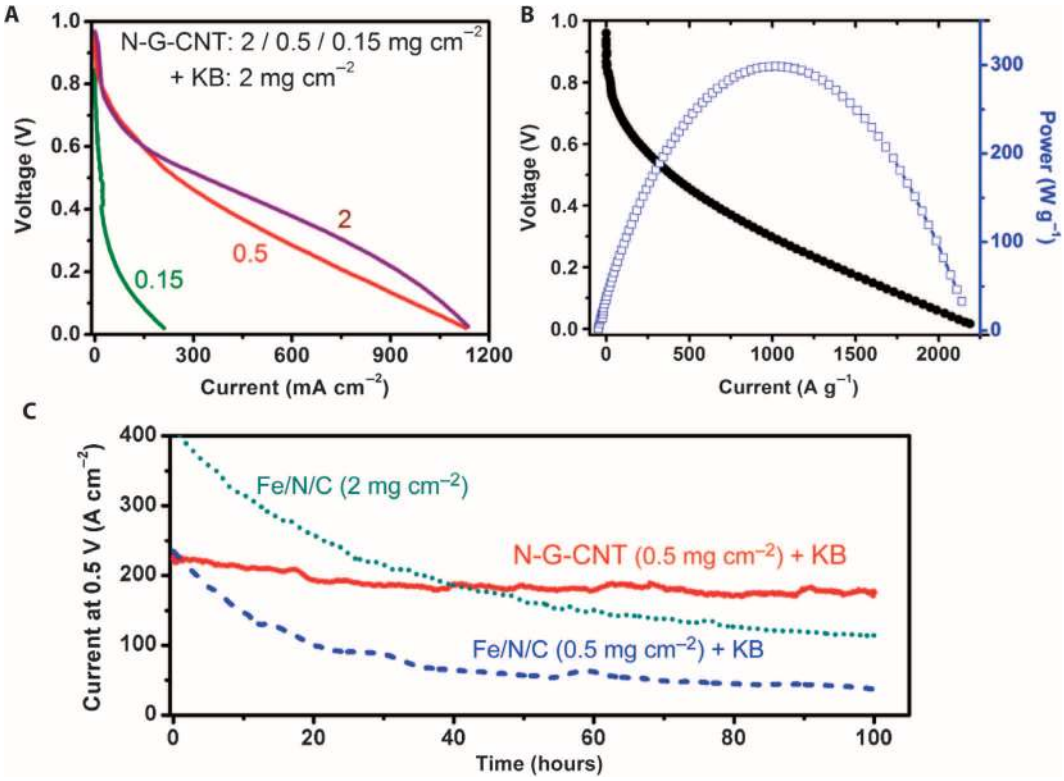

Fig. 7. Power and durability performance of N-G-CNT with the addition of KB in PEM fuel cells. (**A**) Polarization curves of N-G-CNT with loadings: 2, 0.5, or 0.15 mg cm^{-2} plus KB (2 mg cm^{-2}) for each cathode. Weight ratio of (N-G-CNT/KB)/Nafion, 1:1. (**B**) Cell polarization and power density as a function of gravimetric current for N-G-CNT/KB (0.5/2 mg cm^{-2}) with a 1:1 weight ratio of (N-G-CNT/KB)/Nafion. (**C**) Durability of the metal-free N-G-CNT in a PEM fuel cell measured at 0.5 V, compared with a Fe/N/C catalyst. Catalyst loading of N-G-CNT/KB (0.5 mg cm^{-2}) and Fe/N/C (0.5 and 2 mg cm^{-2}). Test conditions: H_2/O_2; 80°C; 100% relative humidity; back pressure, 2 bar. [From J. Shui, M. Wang, F. Du, L. Dai, N-doped carbon nanomaterials are durable catalysts for oxygen reduction reaction in acidic fuel cells. *Sci. Adv.* **1**, e1400129 (2015). Reprinted with permission from AAAS.]

used, ORR and OER are involved in a variety of metal-air batteries during discharge and charge processes, respectively. As such, catalysts play a major role in the electrochemical reduction of O_2 in metal-air batteries with aqueous and nonaqueous media (*35*, *133*–*136*), and hence, it is important to study ORR in metal-air cells.

Because of their high theoretical energy density, Li-air batteries, particularly those utilizing nonaqueous electrolytes with substantially high capacities, have been the main focus of recent research efforts (*2*, *133*). However, the Zn-air battery technology is of particular interest because of its significantly lower cost and much better safety than its Li counterpart. In an aqueous Li-air battery, oxygen is reduced to hydroxyl ions (or hydroperoxide ions) during discharge to combine with Li ions from the anode into soluble LiOH. The overall reaction that occurs at the three-phase zone (Fig. 8A) in a Li-air battery is given in Eq. 5:

$$2Li + 1/2O_2 + H_2O \Leftrightarrow 2LiOH(E^{\theta} = 3.2\ V) \quad (5)$$

For a Zn-air battery, similar reactions occur at the air electrode, but Zinc ions from the anode can combine with hydroxyl ions to form zincate ions $[Zn(OH)_4^{2-}]$, which may decompose to produce ZnO:

$$Zn + 1/2O_2 \Rightarrow ZnO(E^{\theta} = 1.65\ V) \quad (6)$$

In a nonaqueous electrolyte, O_2 enters the porous cathode, is reduced, and then combines with the Li^+ ions in the electrolyte to form solid Li_2O_2 (or Li_2O) on discharge (Fig. 8B). The process is reversed on charging in the rechargeable batteries. Typically, the solid Li_2O_2 is insoluble and accumulates in the pores of the O_2-breathing cathode:

$$2Li + O_2 \Leftrightarrow Li_2O_2(E^{\theta} = 2.96\ V) \text{ or } 2Li + 1/2O_2 \Leftrightarrow Li_2O(E^{\theta} = 2.91\ V) \quad (7)$$

To eliminate the effects of other constituents in air (for example, H_2O, CO_2, and N_2), most studies of Li-air batteries have focused on examining battery performance with pure oxygen gas.

Carbon electrocatalysts for nonaqueous Li-air batteries

In 1996, Abraham and Jiang (*137*) developed a nonaqueous thin film battery consisting of a thin Li metal foil anode, a thin solid polymer electrolyte, and a thin carbon composite electrode. These authors found that the porous carbon electrode with a large surface area could efficiently reduce oxygen from the environment during discharge to generate a high specific capacity of 1410 mAh g^{-1}. Subsequently, various carbon materials, including carbon aerogel, porous carbon, CNT, and graphene, have been investigated as porous cathodes in Li-O_2 batteries (*137*–*139*). During the discharge process, the carbon skeleton acted as an electronically conductive pathway for ORR reaction, whereas the porous structure facilitated the oxygen diffusion to the carbon-electrolyte interface as well as the formation and accumulation of lithium oxides. During the charge process, the carbon skeleton promoted the electrochemical

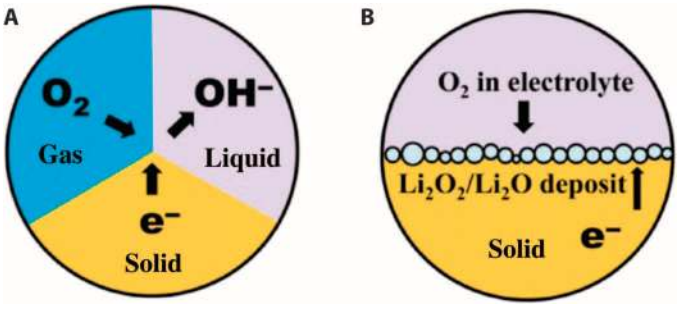

Fig. 8. Illustrated interfaces of air electrodes and proposed electrode structures. (**A**) Gas-solid-liquid three-phase interface model in aqueous electrolytes. (**B**) Liquid-solid two-phase interface model in nonaqueous electrolytes. [From F. Cheng, J. Chen, Metal–air batteries: From oxygen reduction electrochemistry to cathode catalysts. *Chem. Soc. Rev.* **41**, 2172–2192 (2012). Reprinted with permission from the Royal Society of Chemistry.]

decomposition of lithium oxides. Therefore, the porous air electrode plays an important role in achieving high discharge capacity and cycling stability. Generally speaking, the specific capacity of Li-air batteries depends strongly on the pore size, pore volume, and chemical structure of carbon materials (*137*–*139*). It is commonly believed that the discharge process is being terminated when the entire pore volume of the air electrode is filled with lithium oxides, which blocks the O_2 intake. It has been found that only a fraction of the total pore volume (typically less than 50%) has been filled with the product at the end of discharge as micropores, and some of the mesopores would be blocked by lithium oxides formed through reduction of O_2 at the beginning of discharge (*3*, *140*, *141*). In this context, Tran *et al.* (*141*) revealed that the capacity of a gas diffusion electrode (GDE) in a nonaqueous electrolyte depended almost linearly on the average pore diameter of the porous carbon electrode, leading to a quantitative estimation of the electrode capacity.

3D carbon foam with bimodal mesopores of narrow pore size distributions (~4.3 and 30.4 nm), prepared by using a mesocellular silica foam as the hard template, was demonstrated to show an approximately 40% higher discharge capacity in a Li-O_2 battery than the commercial carbon blacks (such as XC-72, Super P), as the ultra-large surface area of mesoporous carbon with a large pore volume could allow a high uptake of lithium oxide during the discharge process (*142*). Template-synthesized porous honeycomb-like carbon with hierarchical pores has also been used as an air electrode in Li-O_2 batteries to yield a significantly higher specific capacity of 3233 mAh g^{-1} and an improved cycle efficiency with a higher discharge voltage plateau (2.75 versus 2.50 V) than that of a conventional carbon electrode (*143*). These results indicate that carbon with an optimal pore structure, a large surface area, and a high pore volume is a desirable air cathode for a high rate and large discharge capacity. Indeed, hierarchical carbon electrodes composed of highly aligned CNT fibrils with a well-defined pore structure, which renders good accessibility of oxygen to the inner electrode and a uniform deposition of discharge products on the individual CNTs, have been demonstrated to significantly enhance both the cycling stability and rate capability for Li-O_2 batteries (*144*). Similarly, NCNTs synthesized on nickel foams by a floating catalyst CVD method were shown to deliver a specific capacity of 1814 mAh g^{-1} (normalized to the weight of the air electrode) in Li-O_2 batteries. These 3D network structures could not only facilitate the O_2 diffusion but also provide sufficient void volume for product deposition during a discharge process. The intimate contact between the NCNTs and the Ni current collector is an additional advantage for suppressing the volume expansion, leading to less polarization and good cycling performance (*143*). On the other hand, Zhang and Zhou (*145*) have designed, along with a conventional air electrode (Fig. 9A), a network gel consisting of SWNTs and ionic liquid [that is, 1-ethyl-3-methylimidazolium bis(trifluoromethylsulfonyl) ([C2C1im][NTf2])] as the oxygen electrode (Fig. 9, B and C) for a Li-O_2 battery. The use of ionic liquid with excellent nonvolatility, high hydrophobicity, high thermal stability, and a broad electrochemical window, in conjunction with the 3D physically cross-linked SWNTs for efficient electron transfer and high uptake of discharge products (Fig. 9C), ensured an efficient tricontinuous pathway for electron, ion, and oxygen transfers (Fig. 9D), leading to a pronounced specific energy density and robust cycling stability without decomposition of the electrolyte (*145*).

In addition to the CNT-based air electrodes, graphene nanosheets (GNSs) have also been extensively studied as the cathode materials for Li-O_2 batteries, showing an excellent electrochemical performance with a discharge capacity up to 8705.9 mAh g^{-1} (*146*). Furthermore, higher average discharge plateau voltage and charge capacity have been observed for the GNS electrode with respect to BP-2000 and Vulcan XC-72 electrodes. Although the detailed mechanism for ORR on GNSs in a nonaqueous electrolyte is still not fully understood, the GNSs are expected to form a 3D electrochemical interface with unique diffusion channels for the electrolyte and O_2 to facilitate the catalytic reaction. In addition, the active sites at the graphene edge could also significantly enhance the ORR electrocatalytic activity (*62*, *63*). In a similar but independent study, Xiao *et al.* (*146*) devised a novel air electrode consisting of a hierarchical arrangement of functionalized GNSs, demonstrating an exceptionally high capacity of 15,000 mAh g^{-1} in Li-O_2 batteries. The observed excellent battery performance was attributed to a unique bimodal porous structure of the GNS electrode, in which microporous channels facilitated rapid O_2 diffusion, whereas the highly connected pores provided a high density of reactive sites for lithium oxide reactions. In addition, defects and functional groups on the graphene sheet promoted the formation of isolated lithium oxide nanoparticles to prevent the air electrode from air blocking.

The efficient oxidization of solid Li_2O_2 through OER during the charging process is highly desirable for rechargeable nonaqueous Li-O_2 batteries. Modeling studies showed that bulk Li_2O_2 had both ionic and electronic conductivities (*147*) and that Li_2O_2 could be effectively decomposed through self-oxidation. However, an in situ transmission electron microscopic study revealed that oxidation of electrochemically deposited Li_2O_2 particles supported on multiwalled CNTs (MCNTs) occurred preferentially at the MCNT/Li_2O_2 interface, which was relatively easy in the initial stage of charging, but became increasingly difficult for the vast majority of Li_2O_2 away from the electrode surface. The oxidation of Li_2O_2 is associated with severe polarization, as indicated by the inexorable increases in charging voltage (*148*). This suggests that the oxidation kinetics at high rates are ultimately limited by the sluggish electron transport in Li_2O_2, leading to large overpotentials (*149*). Under such high overpotentials, the stability of carbon and the possible effect of carbon on electrolyte decomposition are major concerns for the rechargeable nonaqueous Li-O_2 battery. Ottakam Thotiyl and co-workers (*150*) revealed a potential-dependent carbon decomposition and electrolyte decomposition. It was further found that the decomposition of carbon to Li_2CO_3 only occurred on charging above

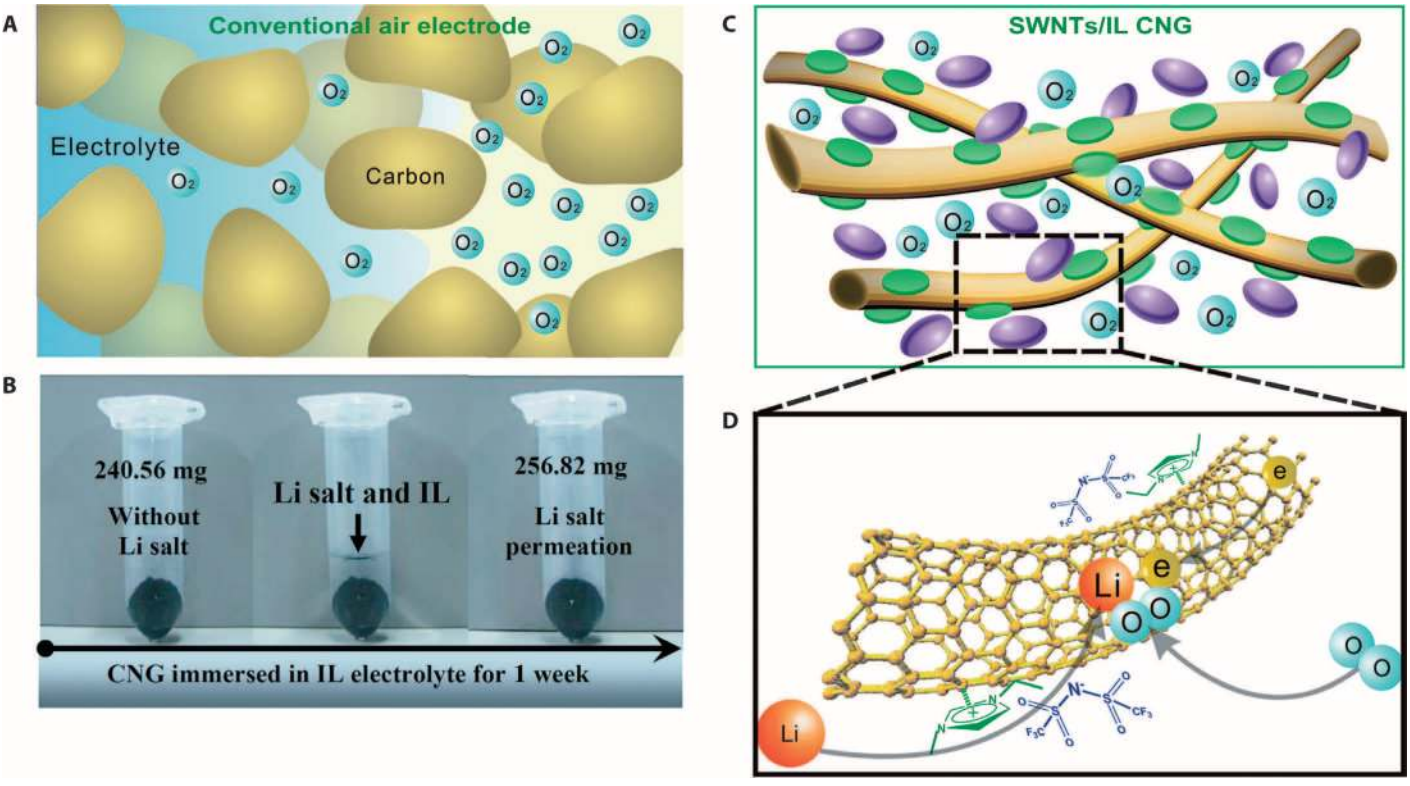

Fig. 9. Comparison of a conventional air electrode and a CNT/ionic liquid–based air electrode. (**A**) Schematic illustration of a conventional air electrode. (**B**) Weight variation of the SWNT/[C2] salt and [C2C1im][NTf_2] for 1 week. (**C** and **D**) Schematic illustration of the SWNT/[C2C1im][NTf2] CNG air electrode, in which SWNTs are untangled through π-π interaction with the imidazolium cation of [C2C1im] (green), whereas [NTf2] ions (purple) are anchored in the gel through electric neutrality (C) and the tricontinuous passage of electrons, ions, and oxygen in SWNT/[C2C1im][NTf2] CNG (D). Electrons conduct along the CNTs, whereas lithium ions transferred from the ionic liquid electrolyte outside into the cross-linked network gel become coordinated by the inside-anchored [NTf_2] ion. Oxygen in the cross-linked network gel is incorporated with the lithium ions and electrons along the SWNTs, thereby turning into the discharge products. [From T. Zhang, H. Zhou, From Li–O_2 to Li–air batteries: Carbon nanotubes/ionic liquid gels with a tricontinuous passage of electrons, ions, and oxygen. *Angew. Chem. Int. Ed.* **51**, 11062–11067 (2012). Reprinted with permission from Wiley.]

3.5 V (versus Li/Li^+), whereas carbon promoted electrolyte (for example, dimethyl sulfoxide and tetraglyme electrolytes) decomposition to Li_2CO_3 and Li carboxylates during discharge and charge processes. Carbon with a hydrophobic surface was found to be less catalytically active toward electrolyte decomposition and, thus, more stable than its hydrophilic counterpart. It is worth noting that only a small proportion of the total carbon decomposition during cycling can be ascribed to the direct chemical reaction with Li_2O_2, whereas the accumulation of Li_2CO_3 on cycling often results in electrode passivation and capacity fading.

These issues could be alleviated by using desirable electrodes with a large specific surface to maximize the Li_2O_2/electrode interfacial area and high electronic conductivity to facilitate electron transport to the reaction sites. To efficiently oxidize bulk Li_2O_2, a redox mediator has been incorporated into the electrolyte to enhance electron-hole transfer between the electrode and Li_2O_2 (*148*). Recent studies have revealed that the application of catalysts, metal-based and/or metal-free heteroatom-doped carbon catalysts, could effectively decrease the recharge overpotential of a Li-O_2 battery compared with pure carbon electrodes (*151*–*154*), as indicated by the N-doped carbon-based ORR/OER bifunctional catalyst (*30*, *155*, *156*). More specifically, we have recently developed vertically aligned N-doped coral-like carbon nanofiber (VA-NCCF) arrays with a large interfacial area and good electronic conductivity by CVD as a binder-free ORR/OER bifunctional electrode for nonaqueous Li-O_2 batteries (*155*). The Li-O_2 battery exhibited an energy efficiency as high as 90% and a narrow voltage gap of 0.3 V between discharge/charge plateaus. Because of the low overpotential of the VA-NCCF electrode, the electrolyte decomposition could be minimized. Excellent cycle ability, high specific capacity (up to 1000 mAh g^{-1}) per cycle, and good reversibility were also demonstrated for the VA-NCCF electrode, attributable to its unique vertically aligned, coral-like N-doped carbon microstructure with a large surface area, high catalytic activity, and optimized oxygen/electron transportation capability. These results demonstrate that highly efficient and reversible Li-O_2 batteries are feasible by using a rationally designed carbon-based oxygen electrode.

Carbon electrocatalysts for aqueous/hybrid Li-air batteries

For the aqueous Li-air battery, the presence of water requires a protective layer on the Li anode to prevent lithium metal from reacting with water. An aqueous electrolyte is used at the cathode (air) side, which is separated from lithium metal by a solid-state electrolyte [a lithium super-ion conductor glass film (LISICON)]. The interface between lithium and LISICON is filled with a thin buffer (electrolyte) polymer to prevent reduction of the solid electrolyte (*135*, *139*, *157*, *158*).

Figure 10 shows the typical configuration of a hybrid Li-air battery, in which N-doped GNSs are used as an air electrode (*158*). For the cathode side with aqueous electrolytes, the knowledge from conventional ORR catalysts may be straightforwardly applied. So far, however, only a few studies have been done on the use of carbon electrocatalysts in aqueous or hybrid Li-O_2 cells (*159*). Owing to the presence of edge defect sites in GNSs, the metal-free GNS air electrodes in hybrid Li-air batteries showed a comparable and even superior discharge voltage to that of the 20 wt % Pt/C (*159*). It was further found that proper thermal treatment of graphene sheets could enhance the catalytic activity toward ORR and also improve the cycling stability. This is because the thermal treatment can remove adsorbed functional groups and improve the graphitization degree of the GNS electrodes.

Carbon electrocatalysts for Zn-air batteries

Due to its high theoretical energy density, excellent safety, and a relatively low cost, Zn-air batteries may overtake the Li-air batteries in the race to the technological marketplace (*133*). Similar reactions at the air electrodes are involved in both the Li-air and Zn-air batteries, as shown in Eqs. 5 to 7.

The formation of soluble products [for example, $Zn(OH)_4^{2-}$, compare Eq. 6] in a Zn-air battery could avoid cathode clogging and volume expansion. Like in an aqueous or a hybrid Li-air battery, the porous air electrode is also attractive for a Zn-air battery (*157*). As discussed earlier, various heteroatom-doped carbons have exhibited robust catalytic activities toward ORR, although only a few studies demonstrate their applications in a whole Zn-air battery (*160*). As an example, NCNTs derived from ethylenediamine precursors were investigated as an air cathode catalyst in Zn-air batteries, which showed a high ORR activity with a cell power density of ~70 mW cm^{-2} at an air-cathode catalyst loading of 0.2 mg cm^{-2} in 6 M KOH (*161*). Likewise, a Zn-air battery based on mesoporous and macroporous N-doped carbon fibers with a high surface area (1271 m^2 g^{-1}) exhibited a peak power density of 194 mW cm^{-2}, comparable to its Pt/C counterpart (192 mWcm^{-2}) (*162*).

Bifunctional catalysts, which have the ability to catalyze both ORR and OER in aqueous media, are highly desirable for rechargeable Zn-air batteries. Noble metal and nonprecious metal catalysts, such as metal oxides supported by carbon, have long been investigated in aqueous electrolytes as bifunctional catalysts to facilitate ORR and OER (*163*–*165*). In contrast, carbon-based metal-free bifunctional catalysts are a recent development (*15*, *30*, *156*, *166*). Through polymerization of aniline in the presence of phytic acid to produce polyaniline (PANi) aerogels (*167*) and subsequent pyrolysis, we have recently produced 3D N and P co-doped mesoporous nanocarbon (NPMC) foams that have a surface area of up to ~1663 m^2 g^{-1} and good electrocatalytic properties for both ORR and OER (*30*). When used as air electrodes for primary batteries, the NPMC-based Zn-air batteries showed an open circuit potential of 1.48 V, a specific capacity of 735 mAh g_{Zn}^{-1} (corresponding to an energy density of 835 Wh kg_{Zn}^{-1}), and a peak power density of 55 mW cm^{-2}, and could sustain stable operation for 240 hours after mechanical recharging (*30*). In addition, two-electrode rechargeable batteries based on the NPMC-1000 (pyrolysis temperature: 1000°C) air electrode could be stably cycled for 180 cycles at 2 mA cm^{-2} (Fig. 11A). Although NPMC-1000 accelerates both ORR and OER, a certain degree of irreversibility is unavoidable because of the different catalytic activities of the same catalyst toward ORR and OER reactions. Consequently, a deteriorating performance was observed for the two-electrode rechargeable Zn-air battery during a long-term cycling test. Therefore, to further improve the NPMC battery performance, we have also constructed a three-electrode rechargeable Zn-air battery (Fig. 11B), in which the NPMC bifunctional catalysts are prevented from being contacted with the oxidative (or reductive) potential during ORR (or OER), to study the electrocatalytic activities of the NPMC foam for both OER and ORR independently. In this case, the activities toward ORR and OER could be independently regulated by adjusting the catalyst mass loading on each of the two air electrodes, and a balanced reversible transfer between oxygen reduction and evolution was readily achieved. Figure 11C shows the discharge and charge polarization curves for the three-electrode batteries with various air electrodes. The three-electrode rechargeable Zn-air battery using NPMC-1000 as air electrodes showed no obvious voltage change over 600 discharge/charge cycles (for 100 hours, Fig. 11D), comparable to that of a three-electrode Zn-air battery using the state-of-the-art Pt/C and RuO_2 as the ORR and OER catalysts, respectively (*30*). The Zn-air battery based on the NPMC air electrodes is comparable to, or even better than, most of the recently reported rechargeable Zn-air batteries based on metal/metal oxide electrodes (*165*, *168*–*170*). To gain insights into the ORR and OER catalytic mechanisms of the NPMC metal-free bifunctional catalysts, we performed the first-principles calculations using the DFT methods to determine the electronic structures and catalytic reactions for the N, P co-doped carbon structures. Our calculations revealed that the N, P co-doping and the graphene edge effect are crucial for the bifunctional electrocatalytic activities of our NPMC materials (*30*).

More generally, it is critical to establish design principles or descriptors for heteroatom-doped carbon nanomaterials based on computational modeling. It has been shown that in ORR and OER, surface-oxygen bond energy is closely related to the charge densities on graphene around dopants because the reaction intermediates (*OH, *O, *OOH, where the asterisk indicates a bond to the surface) interact with the surface through an O atom. Thus, electrochemical quantities, such as $4e^-$ pathway selectivity and onset potential, should relate well to the binding strength of intrinsic oxygen-containing intermediates (adsorbed species) on the catalyst surface. To derive the minimum overpotential (corresponding to the highest activity) in doped graphene systems, the overpotentials were calculated for different re-

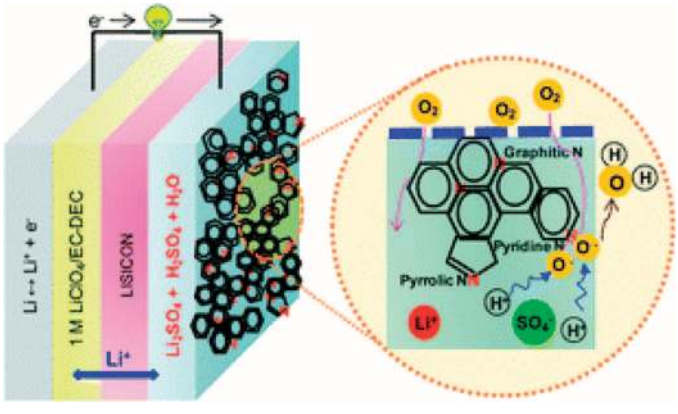

Fig. 10. Schematic representation of a hybrid Li-air battery. The enlarged image shows the basic reaction process in the air electrode based on NG. [From E. Yoo, J. Nakamura, H. Zhou, N-Doped graphene nanosheets for Li–air fuel cells under acidic conditions. *Energy Environ. Sci.* **5**, 6928–6932 (2012). Reprinted with permission from the Royal Society of Chemistry.]

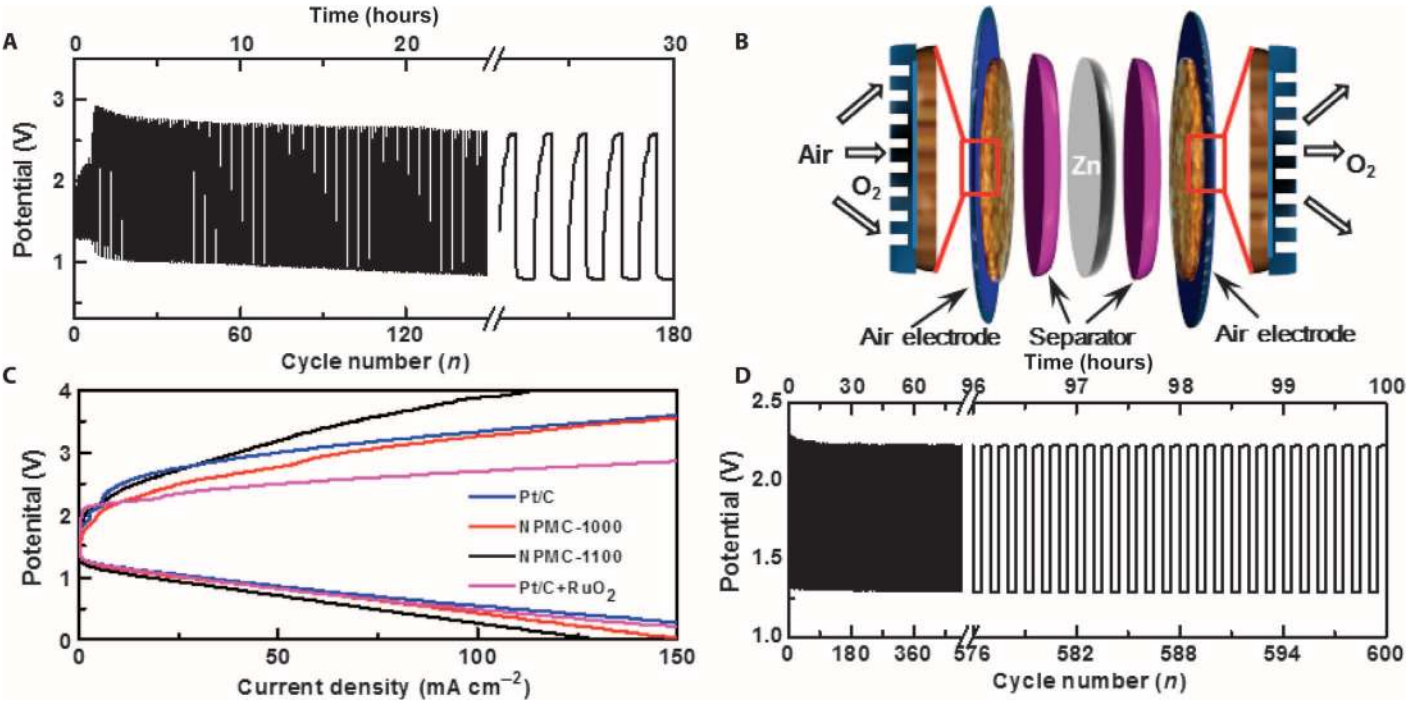

Fig. 11. Performance of rechargeable Zn-air batteries. (**A**) Discharge/charge cycling curves of a two-electrode rechargeable Zn-air battery at a current density of 2 mA cm^{-2} using the NPMC-1000 (pyrolysis at 1000°C) air electrode. Three-electrode Zn-air batteries. (**B**) Schematic illustration for the basic configuration of a three-electrode Zn-air battery by coupling a Zn electrode with two air electrodes to separate ORR and OER. The enlarged parts illustrate the porous structures of the air electrodes, which facilitates the gas exchange. (**C**) Charge and discharge polarization curves of three-electrode Zn-air batteries using the NPMC-1000, NPMC-1100, or commercial Pt/C catalyst as both of the air electrodes, along with the corresponding curve (that is, Pt/C + RuO_2) for the three-electrode Zn-air battery with Pt/C and RuO_2 nanoparticles as each of the air electrodes, respectively. (**D**) Discharge/charge cycling curves of a three-electrode Zn-air battery using NPMC-1000 as air electrodes (0.5 mg cm^{-2} for ORR and 1.5 mg cm^{-2} for OER) at a current density of 2 mA cm^{-2}. [From J. Zhang, Z. Zhao, Z. Xia, L. Dai, A metal-free bifunctional electrocatalyst for oxygen reduction and oxygen evolution reactions. *Nat. Nanotechnol.* **10**, 444–452 (2015). Reprinted with permission from the Nature Publishing Group.]

action sites on different structures using the adsorption energy difference between *O and *OH for OER and adsorption energy of *OH for ORR, following the approaches outlined by Nørskov *et al.* (*171*, *172*) and Man *et al.* (*172*). When a descriptor is identified, the catalytic rates typically have a "volcano"-shaped dependence on the descriptor with a maximum at the optimum value of this descriptor. Various material structures have been calculated, including NG quantum dots (*173*); NG ribbons (*174*); N, S, O, B single-doped graphene (*175*); and P, N co-doped graphene (*30*). Through these calculations, key descriptors were identified for both ORR and OER on these catalysts, showing that the free energy difference between *OH and *OOH has a linear relationship over all the sites. It is worth noting that OER and ORR with the minimum overpotentials can occur near the edge on the same graphitic structure but different sites. Therefore, as mentioned earlier, the combined experimental and theoretical approach should facilitate the design and development of metal-free, carbon-based catalysts with controlled locations and structures of the active centers, and hence tailor-made electrocatalytic activities for energy conversion and storage in fuel cells, metal-air batteries, and many other energy-related devices/systems.

As can be seen from the preceding discussion, a variety of heteroatom-doped carbons with a large surface area, good electrical conductivity, and tunable pore structure have been rationally designed and fabricated for various promising applications. Porous carbons with hierarchical porosities can facilitate oxygen/electrolyte/electron transports and enhance solid oxide deposition in metal-air batteries during the discharging process. Therefore, in addition to the demonstration of high ORR catalytic activities for carbon nanostructures, the recent development of ORR and OER bifunctional nanocarbon catalysts is important to the metal-air rechargeable battery technology. With carbon nanomaterials of various heteroatom-doped multidimensional architectures as the air cathode for ORR/OER, high-performance Li-air and Zn-air primary and rechargeable batteries have been developed. Despite these recent advancements, in-depth theoretical and experimental studies are needed to understand the bifunctional electrocatalytic mechanisms of these novel electrocatalysts, which should facilitate the development of multifunctional carbon nanomaterials for other electrocatalytic applications as well.

CONCLUDING REMARKS

The importance of developing renewable energy technologies has been evident from the fact that global energy consumption, along with "greenhouse" gas emission, has been accelerating at an alarming rate. Fuel cells and metal-air batteries are among the most efficient and environmentally benign energy conversion and storage technologies to meet the demand for alternative energy sources. However, noble metal (for example, platinum) and/or metal oxide catalysts are required to

catalyze the key chemical reactions, including ORR and OER, in fuel cells and metal-air batteries. The high cost, low selectivity, poor durability, and detrimental environmental effects intrinsically associated with most of the metal-based catalysts have been shown to be the major "showstopper" to mass-market fuel cells or metal-air batteries for commercial applications. Along with the intensive research efforts in reducing or replacing (noble) metal-based catalysts, a new class of metal-free ORR catalysts based on carbon nanomaterials doped with heteroatom(s) has been recently discovered. With rapid advances in carbon nanomaterials and nanotechnology, various heteroatom-doped carbon nanostructures, including CNTs, graphene and derivatives, and 3D porous carbon foams, have been successfully developed as low-cost, highly efficient, metal-free electrocatalysts for ORR and OER in fuel cells and metal-air batteries.

In fuel cells, various metal-free ORR catalysts based on heteroatom-doped carbon nanomaterials have been demonstrated to exhibit a high electrocatalytic activity, a good tolerance to fuel crossover/CO poisoning effect, and an excellent operation durability comparable to or even better than that of the best nonprecious metal catalysts, opening avenues for clean energy generation from affordable and durable fuel cells (for example, PEMFCs). On the other hand, a variety of metal-free porous carbons have been investigated as air electrodes in nonaqueous Li-air batteries. Porous carbons with hierarchical porosities could ensure an efficient oxygen/electrolyte transport, a high uptake of the solid lithium oxide produced in the discharging process, and a good electric conductivity for fast electron conduction. Bifunctional catalysts are essential for the development of rechargeable batteries. Very recently, metal-free, carbon-based ORR and OER bifunctional electrocatalysts have been developed as efficient air electrodes for primary and rechargeable Zn-air batteries, showing a high specific capacity, good cycling rate capability, and long operation stability.

Despite the great success that has been achieved in the design and development of various heteroatom-doped, metal-free carbon-based electrocatalysts for ORR and OER, they still suffer from some inherent drawbacks, including the low concentration of heteroatom dopants, relatively poor catalytic performance in acidic media, and difficulties in controlling the exact locations and structures of active sites. Although it is still a challenge to experimentally study the active sites, the first-principles approach has been used as an alternative and powerful tool to study the catalytic mechanism of heteroatom-doped carbon nanomaterials as efficient catalysts for ORR in fuel cells and OER in metal-air batteries. The theoretical investigations complement state-of-the-art experimental techniques, especially in cases where experimental characterization of a variety of intermediates is difficult or impossible. The electronic structures, active sites, reaction pathways, and energy barriers have been studied using DFT methods. To rationally design a catalyst, however, it is critical to understand which intrinsic material characteristics (or descriptors) control catalysis. Continued research with the combined experimental and theoretical approach should lead to the development of highly efficient carbon-based catalysts for fuel cells and metal-air batteries in a time- and cost-saving manner, which will affect every aspect of our daily life in the near future.

MATERIALS AND METHODS

To demonstrate the evaluation methods of electrocatalytic activity toward ORR by using RDE and RRDE (Fig. 1, A and B), the commercially available Pt/C catalyst (C2-20, 20% platinum on Vulcan XC-72R; E-TEK) was used as an electrocatalyst for ORR and measured in 0.1 M KOH. The electrochemical performance was characterized in a three-electrode configuration with the RDE or RRDE. The potential, measured against an Ag/AgCl electrode, was converted to potential versus RHE according to $E_{\text{vs RHE}} = E_{\text{vs Ag/AgCl}} + E_{\text{ø Ag/AgCl}} + 0.059$ pH. To prepare the working electrode, 5 mg of Pt/C catalyst was dispersed in an aqueous solution containing 0.95 ml of deionized water and 0.05 ml of 5 wt % Nafion under sonication. The obtained homogeneous catalyst ink (6 μl) was dropped onto a mirror-polished glassy carbon electrode to achieve a mass loading of 0.15 mg cm^{-2}. A 0.1 M KOH aqueous solution saturated with oxygen was used as the electrolyte.

REFERENCES AND NOTES

1. B. Dunn, H. Kamath, J.-M. Tarascon, Electrical energy storage for the grid: A battery of choices. *Science* **334**, 928–935 (2011).
2. F. Cheng, J. Chen, Metal–air batteries: From oxygen reduction electrochemistry to cathode catalysts. *Chem. Soc. Rev.* **41**, 2172–2192 (2012).
3. J. Zhang, C. M. Li, Nanoporous metals: Fabrication strategies and advanced electrochemical applications in catalysis, sensing and energy systems. *Chem. Soc. Rev.* **41**, 7016–7031 (2012).
4. S. Zhang, Y. Shao, G. Yin, Y. Lin, Recent progress in nanostructured electrocatalysts for PEM fuel cells. *J. Mater. Chem. A* **1**, 4631–4641 (2013).
5. J. Suntivich, H. A. Gasteiger, N. Yabuuchi, H. Nakanishi, J. B. Goodenough, Y. Shao-Horn, Design principles for oxygen-reduction activity on perovskite oxide catalysts for fuel cells and metal–air batteries. *Nat. Chem.* **3**, 546–550 (2011).
6. Y. Jiao, Y. Zheng, M. Jaroniec, S. Z. Qiao, Design of electrocatalysts for oxygen- and hydrogen-involving energy conversion reactions. *Chem. Soc. Rev.* **44**, 2060–2086 (2015).
7. K. Gong, F. Du, Z. Xia, M. Durstock, L. Dai, Nitrogen-doped carbon nanotube arrays with high electrocatalytic activity for oxygen reduction. *Science* **323**, 760–764 (2009).
8. L. Dai, Y. Xue, L. Qu, H.-J. Choi, J.-B. Baek, Metal-free catalysts for oxygen reduction reaction. *Chem. Rev.* **115**, 4823–4892 (2015).
9. L. Qu, Y. Liu, J.-B. Baek, L. Dai, Nitrogen-doped graphene as efficient metal-free electrocatalyst for oxygen reduction in fuel cells. *ACS Nano* **4**, 1321–1326 (2010).
10. Z. Yang, Z. Yao, G. Li, G. Fang, H. Nie, Z. Liu, X. Zhou, X. Chen, S. Huang, Sulfur-doped graphene as an efficient metal-free cathode catalyst for oxygen reduction. *ACS Nano* **6**, 205–211 (2012).
11. S. Chen, J. Bi, Y. Zhao, L. Yang, C. Zhang, Y. Ma, Q. Wu, X. Wang, Z. Hu, Nitrogen-doped carbon nanocages as efficient metal-free electrocatalysts for oxygen reduction reaction. *Adv. Mater.* **24**, 5593–5597 (2012).
12. I.-Y. Jeon, S. Zhang, L. Zhang, H.-J. Choi, J.-M. Seo, Z. Xia, L. Dai, J.-B. Baek, Edge-selectively sulfurized graphene nanoplatelets as efficient metal-free electrocatalysts for oxygen reduction reaction: The electron spin effect. *Adv. Mater.* **25**, 6138–6145 (2013).
13. R. Liu, D. Wu, X. Feng, K. Müllen, Nitrogen-doped ordered mesoporous graphitic arrays with high electrocatalytic activity for oxygen reduction. *Angew. Chem. Int. Ed.* **49**, 2565–2569 (2010).
14. L. Feng, Y. Yan, Y. Chen, L. Wang, Nitrogen-doped carbon nanotubes as efficient and durable metal-free cathodic catalysts for oxygen reduction in microbial fuel cells. *Energy Environ. Sci.* **4**, 1892–1899 (2011).
15. B. Winther-Jensen, D. R. MacFarlane, New generation, metal-free electrocatalysts for fuel cells, solar cells and water splitting. *Energy Environ. Sci.* **4**, 2790–2798 (2011).
16. Y. Zheng, Y. Jiao, J. Chen, J. Liu, J. Liang, A. Du, W. Zhang, Z. Zhu, S. C. Smith, M. Jaroniec, G. Q. Lu, S. Z. Qiao, Nanoporous graphitic-C_3N_4@carbon metal-free electrocatalysts for highly efficient oxygen reduction. *J. Am. Chem. Soc.* **133**, 20116–20119 (2011).
17. M. Zhang, L. Dai, Carbon nanomaterials as metal-free catalysts in next generation fuel cells. *Nano Energy* **1**, 514–517 (2012).
18. L. Yang, S. Jiang, Y. Zhao, L. Zhu, S. Chen, X. Wang, Q. Wu, J. Ma, Y. Ma, Z. Hu, Boron-doped carbon nanotubes as metal-free electrocatalysts for the oxygen reduction reaction. *Angew. Chem. Int. Ed.* **50**, 7132–7135 (2011).
19. Y. Zheng, Y. Jiao, L. Ge, M. Jaroniec, S. Z. Qiao, Two-step boron and nitrogen doping in graphene for enhanced synergistic catalysis. *Angew. Chem. Int. Ed.* **52**, 3110–3116 (2013).
20. S. Wang, L. Zhang, Z. Xia, A. Roy, D. W. Chang, J.-B. Baek, L. Dai, BCN graphene as efficient metal-free electrocatalyst for the oxygen reduction reaction. *Angew. Chem. Int. Ed.* **51**, 4209–4212 (2012).
21. I.-Y. Jeon, H.-J. Choi, M. Choi, J.-M. Seo, S.-M. Jung, M.-J. Kim, S. Zhang, L. Zhang, Z. Xia, L. Dai, N. Park, J.-B. Baek, Facile, scalable synthesis of edge-halogenated graphene nanoplatelets

as efficient metal-free eletrocatalysts for oxygen reduction reaction. *Sci. Rep.* **3**, 1810 (2013).
22. D. Geng, N. Ding, T. S. Andy Hor, Z. Liu, X. Sun, Y. Zong, Potential of metal-free "graphene alloy" as electrocatalysts for oxygen reduction reaction. *J. Mater. Chem. A* **3**, 1795–1810 (2015).
23. S. Wang, D. Yu, L. Dai, Polyelectrolyte functionalized carbon nanotubes as efficient metal-free electrocatalysts for oxygen reduction. *J. Am. Chem. Soc.* **133**, 5182–5185 (2011).
24. S. Wang, D. Yu, L. Dai, D. W. Chang, J.-B. Baek, Polyelectrolyte-functionalized graphene as metal-free electrocatalysts for oxygen reduction. *ACS Nano* **5**, 6202–6209 (2011).
25. J. Shui, M. Wang, F. Du, L. Dai, N-doped carbon nanomaterials are durable catalysts for oxygen reduction reaction in acidic fuel cells. *Sci. Adv.* **1**, e1400129 (2015).
26. J. Liu, Y. Liu, N. Liu, Y. Han, X. Zhang, H. Huang, Y. Lifshitz, S.-T. Lee, J. Zhong, Z. Kang, Metal-free efficient photocatalyst for stable visible water splitting via a two-electron pathway. *Science* **347**, 970–974 (2015).
27. Y. Zheng, Y. Jiao, Y. Zhu, L. H. Li, Y. Han, Y. Chen, A. Du, M. Jaroniec, S. Z. Qiao, Hydrogen evolution by a metal-free electrocatalyst. *Nat. Commun.* **5**, 3783 (2014).
28. S. Zhang, P. Kang, S. Ubnoske, M. K. Brennaman, N. Song, R. L. House, J. T. Glass, T. J. Meyer, Polyethylenimine-enhanced electrocatalytic reduction of CO_2 to formate at nitrogen-doped carbon nanomaterials. *J. Am. Chem. Soc.* **136**, 7845–7848 (2014).
29. Y. Xue, J. Liu, H. Chen, R. Wang, D. Li, J. Qu, L. Dai, Nitrogen-doped graphene foams as metal-free counter electrodes in high-performance dye-sensitized solar cells. *Angew. Chem. Int. Ed.* **51**, 12124–12127 (2012).
30. J. Zhang, Z. Zhao, Z. Xia, L. Dai, A metal-free bifunctional electrocatalyst for oxygen reduction and oxygen evolution reactions. *Nat. Nanotechnol.* **10**, 444–452 (2015).
31. Y. Zhao, R. Nakamura, K. Kamiya, S. Nakanishi, K. Hashimoto, Nitrogen-doped carbon nanomaterials as non-metal electrocatalysts for water oxidation. *Nat. Commun.* **4**, 2390 (2013).
32. B. Kumar, M. Asadi, D. Pisasale, S. Sinha-Ray, B. A. Rosen, R. Haasch, J. Abiade, A. L. Yarin, A. Salehi-Khojin, Renewable and metal-free carbon nanofibre catalysts for carbon dioxide reduction. *Nat. Commun.* **4**, 2819 (2013).
33. Y. Zheng, Y. Jiao, M. Jaroniec, S. Z. Qiao, Advancing the electrochemistry of the hydrogen-evolution reaction through combining experiment and theory. *Angew. Chem. Int. Ed.* **54**, 52–65 (2015).
34. D. S. Su, S. Perathoner, G. Centi, Nanocarbons for the development of advanced catalysts. *Chem. Rev.* **113**, 5782–5816 (2013).
35. L. Dai, D. W. Chang, J.-B. Baek, W. Lu, Carbon nanomaterials for advanced energy conversion and storage. *Small* **8**, 1130–1166 (2012).
36. J. Liu, Y. Xue, M. Zhang, L. Dai, Graphene-based materials for energy applications. *MRS Bull.* **37**, 1265–1272 (2012).
37. D. Yu, E. Nagelli, F. Du, L. Dai, Metal-free carbon nanomaterials become more active than metal catalysts and last longer. *J. Phys. Chem. Lett.* **1**, 2165–2173 (2010).
38. O. Antoine, R. Durand, RRDE study of oxygen reduction on Pt nanoparticles inside Nafion®: H_2O_2 production in PEMFC cathode conditions. *J. Appl. Electrochem.* **30**, 839–844 (2000).
39. S. K. Zecevic, J. S. Wainright, M. H. Litt, S. Lj. Gojkovic, R. F. Savinell, Kinetics of O_2 reduction on a Pt electrode covered with a thin film of solid polymer electrolyte. *J. Electrochem. Soc.* **144**, 2973–2982 (1997).
40. J. Zhang, C. Guo, L. Zhang, C. M. Li, Direct growth of flower-like manganese oxide on reduced graphene oxide towards efficient oxygen reduction reaction. *Chem. Commun.* **49**, 6334–6336 (2013).
41. K. Suárez-Alcántara, A. Rodríguez-Castellanos, R. Dante, O. Solorza-Feria, $Ru_xCr_ySe_z$ electrocatalyst for oxygen reduction in a polymer electrolyte membrane fuel cell. *J. Power Sources* **157**, 114–120 (2006).
42. U. A. Paulus, T. J. Schmidt, H. A. Gasteiger, R. J. Behm, Oxygen reduction on a high-surface area Pt/Vulcan carbon catalyst: A thin-film rotating ring-disk electrode study. *J. Electroanal. Chem.* **495**, 134–145 (2001).
43. C. Paliteiro, A. Hamnett, J. B. Goodenough, The electroreduction of oxygen on pyrolytic graphite. *J. Electroanal. Chem. Interfacial Electrochem.* **233**, 147–159 (1987).
44. J. Suntivich, K. J. May, H. A. Gasteiger, J. B. Goodenough, Y. Shao-Horn, A perovskite oxide optimized for oxygen evolution catalysis from molecular orbital principles. *Science* **334**, 1383–1385 (2011).
45. V. Ramani, H. R. Kunz, J. M. Fenton, The polymer electrolyte fuel cell. *Electrochem. Soc. Interface* **13**, 17 (2004).
46. J. B. Goodenough, Evolution of strategies for modern rechargeable batteries. *Acc. Chem. Res.* **46**, 1053–1061 (2013).
47. H. Zhang, P. K. Shen, Recent development of polymer electrolyte membranes for fuel cells. *Chem. Rev.* **112**, 2780–2832 (2012).
48. M. K. Debe, Electrocatalyst approaches and challenges for automotive fuel cells. *Nature* **486**, 43–51 (2012).
49. A. Rabis, P. Rodriguez, T. J. Schmidt, Electrocatalysis for polymer electrolyte fuel cells: Recent achievements and future challenges. *ACS Catal.* **2**, 864–890 (2012).
50. R. Jasinski, A new fuel cell cathode catalyst. *Nature* **201**, 1212–1213 (1964).
51. D. S. Su, G. Sun, Nonprecious-metal catalysts for low-cost fuel cells. *Angew. Chem. Int. Ed.* **50**, 11570–11572 (2011).
52. M. Yuasa, A. Yamaguchi, H. Itsuki, K. Tanaka, M. Yamamoto, K. Oyaizu, Modifying carbon particles with polypyrrole for adsorption of cobalt ions as electrocatatytic site for oxygen reduction. *Chem. Mater.* **17**, 4278–4281 (2005).
53. R. Bashyam, P. Zelenay, A class of non-precious metal composite catalysts for fuel cells. *Nature* **443**, 63–66 (2006).
54. G. Wu, K. L. More, C. M. Johnston, P. Zelenay, High-performance electrocatalysts for oxygen reduction derived from polyaniline, iron, and cobalt. *Science* **332**, 443–447 (2011).
55. M. Lefèvre, E. Proietti, F. Jaouen, J.-P. Dodelet, Iron-based catalysts with improved oxygen reduction activity in polymer electrolyte fuel cells. *Science* **324**, 71–74 (2009).
56. Y. Zhao, K. Watanabe, K. Hashimoto, Self-supporting oxygen reduction electrocatalysts made from a nitrogen-rich network polymer. *J. Am. Chem. Soc.* **134**, 19528–19531 (2012).
57. J. R. Pels, F. Kapteijn, J. A. Moulijn, Q. Zhu, K. M. Thomas, Evolution of nitrogen functionalities in carbonaceous materials during pyrolysis. *Carbon* **33**, 1641–1653 (1995).
58. D. S. Su, J. Zhang, B. Frank, A. Thomas, X. Wang, J. Paraknowitsch, R. Schlögl, Metal-free heterogeneous catalysis for sustainable chemistry. *ChemSusChem* **3**, 169–180 (2010).
59. H. Niwa, M. Kobayashi, K. Horiba, Y. Harada, M. Oshima, K. Terakura, T. Ikeda, Y. Koshigoe, J.-i. Ozaki, S. Miyata, S. Ueda, Y. Yamashita, H. Yoshikawa, K. Kobayashi, X-ray photoemission spectroscopy analysis of N-containing carbon-based cathode catalysts for polymer electrolyte fuel cells. *J. Power Sources* **196**, 1006–1011 (2011).
60. P. H. Matter, L. Zhang, U. S. Ozkan, The role of nanostructure in nitrogen-containing carbon catalysts for the oxygen reduction reaction. *J. Catal.* **239**, 83–96 (2006).
61. H. Kim, K. Lee, S. I. Woo, Y. Jung, On the mechanism of enhanced oxygen reduction reaction in nitrogen-doped graphene nanoribbons. *Phys. Chem. Chem. Phys.* **13**, 17505–17510 (2011).
62. W. Yuan, Y. Zhou, Y. Li, C. Li, H. Peng, J. Zhang, Z. Liu, L. Dai, G. Shi, The edge- and basal-plane-specific electrochemistry of a single-layer graphene sheet. *Sci. Rep.* **3**, 2248 (2013).
63. A. Shen, Y. Zou, Q. Wang, R. A. W. Dryfe, X. Huang, S. Dou, L. Dai, S. Wang, Oxygen reduction reaction in a droplet on graphite: Direct evidence that the edge is more active than the basal plane. *Angew. Chem. Int. Ed.* **53**, 10804–10808 (2014).
64. D. Yu, Q. Zhang, L. Dai, Highly efficient metal-free growth of nitrogen-doped single-walled carbon nanotubes on plasma-etched substrates for oxygen reduction. *J. Am. Chem. Soc.* **132**, 15127–15129 (2010).
65. S. Kundu, T. C. Nagaiah, W. Xia, Y. Wang, S. V. Dommele, J. H. Bitter, M. Santa, G. Grundmeier, M. Bron, W. Schuhmann, M. Muhler, Electrocatalytic activity and stability of nitrogen-containing carbon nanotubes in the oxygen reduction reaction. *J. Phys. Chem. C* **113**, 14302–14310 (2009).
66. H. Li, W. Kang, L. Wang, Q. Yue, S. Xu, H. Wang, J. Liu, Synthesis of three-dimensional flowerlike nitrogen-doped carbons by a copyrolysis route and the effect of nitrogen species on the electrocatalytic activity in oxygen reduction reaction. *Carbon* **54**, 249–257 (2013).
67. C. V. Rao, C. R. Cabrera, Y. Ishikawa, In search of the active site in nitrogen-doped carbon nanotube electrodes for the oxygen reduction reaction. *J. Phys. Chem. Lett.* **1**, 2622–2627 (2010).
68. K. A. Kurak, A. B. Anderson, Nitrogen-treated graphite and oxygen electroreduction on pyridinic edge sites. *J. Phys. Chem. C* **113**, 6730–6734 (2009).
69. J. Yan, H. Meng, F. Xie, X. Yuan, W. Yu, W. Lin, W. Ouyang, D. Yuan, Metal free nitrogen doped hollow mesoporous graphene-analogous spheres as effective electrocatalyst for oxygen reduction reaction. *J. Power Sources* **245**, 772–778 (2014).
70. S. Maldonado, K. J. Stevenson, Influence of nitrogen doping on oxygen reduction electrocatalysis at carbon nanofiber electrodes. *J. Phys. Chem. B* **109**, 4707–4716 (2005).
71. J. D. Wiggins-Camacho, K. J. Stevenson, Effect of nitrogen concentration on capacitance, density of states, electronic conductivity, and morphology of N-doped carbon nanotube electrodes. *J. Phys. Chem. C* **113**, 19082 (2009).
72. H. Niwa, K. Horiba, Y. Harada, M. Oshima, T. Ikeda, K. Terakura, J.-i. Ozaki, S. Miyata, X-ray absorption analysis of nitrogen contribution to oxygen reduction reaction in carbon alloy cathode catalysts for polymer electrolyte fuel cells. *J. Power Sources* **187**, 93–97 (2009).
73. Z. Xiang, D. Cao, L. Huang, J. Shui, M. Wang, L. Dai, Nitrogen-doped holey graphitic carbon from 2D covalent organic polymers for oxygen reduction. *Adv. Mater.* **26**, 3315–3320 (2014).
74. Z. Xiang, Y. Xue, D. Cao, L. Huang, J.-F. Chen, L. Dai, Highly efficient electrocatalysts for oxygen reduction based on 2D covalent organic polymers complexed with non-precious metals. *Angew. Chem. Int. Ed.* **53**, 2433–2437 (2014).
75. J. D. Wiggins-Camacho, K. J. Stevenson, Mechanistic discussion of the oxygen reduction reaction at nitrogen-doped carbon nanotubes. *J. Phys. Chem. C* **115**, 20002–20010 (2011).
76. T. Sharifi, G. Hu, X. Jia, T. Wågberg, Formation of active sites for oxygen reduction reactions by transformation of nitrogen functionalities in nitrogen-doped carbon nanotubes. *ACS Nano* **6**, 8904–8912 (2012).
77. Z. Wang, R. Jia, J. Zheng, J. Zhao, L. Li, J. Song, Z. Zhu, Nitrogen-promoted self-assembly of N-doped carbon nanotubes and their intrinsic catalysis for oxygen reduction in fuel cells. *ACS Nano* **5**, 1677–1684 (2011).

78. Z. Chen, D. Higgins, Z. Chen, Nitrogen doped carbon nanotubes and their impact on the oxygen reduction reaction in fuel cells. *Carbon* **48**, 3057–3065 (2010).
79. H. T. Chung, J. H. Won, P. Zelenay, Active and stable carbon nanotube/nanoparticle composite electrocatalyst for oxygen reduction. *Nat. Commun.* **4**, 1922 (2013).
80. Z. Mo, S. Liao, Y. Zheng, Z. Fu, Preparation of nitrogen-doped carbon nanotube arrays and their catalysis towards cathodic oxygen reduction in acidic and alkaline media. *Carbon* **50**, 2620–2627 (2012).
81. R. A. Sidik, A. B. Anderson, N. P. Subramanian, S. P. Kumaraguru, B. N. Popov, O_2 reduction on graphite and nitrogen-doped graphite: Experiment and theory. *J. Phys. Chem. B* **110**, 1787–1793 (2006).
82. J. Masa, A. Zhao, W. Xia, Z. Sun, B. Mei, M. Muhler, W. Schuhmann, Trace metal residues promote the activity of supposedly metal-free nitrogen-modified carbon catalysts for the oxygen reduction reaction. *Electrochem. Commun.* **34**, 113–116 (2013).
83. L. Wang, A. Ambrosi, M. Pumera, "Metal-free" catalytic oxygen reduction reaction on heteroatom-doped graphene is caused by trace metal impurities. *Angew. Chem. Int. Ed.* **52**, 13818–13821 (2013).
84. L. Wang, M. Pumera, Residual metallic impurities within carbon nanotubes play a dominant role in supposedly "metal-free" oxygen reduction reactions. *Chem. Commun.* **50**, 12662–12664 (2014).
85. W. Yang, T.-P. Fellinger, M. Antonietti, Efficient metal-free oxygen reduction in alkaline medium on high-surface-area mesoporous nitrogen-doped carbons made from ionic liquids and nucleobases. *J. Am. Chem. Soc.* **133**, 206–209 (2011).
86. J. Liang, Y. Zheng, J. Chen, J. Liu, D. Hulicova-Jurcakova, M. Jaroniec, S. Z. Qiao, Facile oxygen reduction on a three-dimensionally ordered macroporous graphitic C_3N_4/carbon composite electrocatalyst. *Angew. Chem. Int. Ed.* **51**, 3892–3896 (2012).
87. X. Wang, J. S. Lee, Q. Zhu, J. Liu, Y. Wang, S. Dai, Ammonia-treated ordered mesoporous carbons as catalytic materials for oxygen reduction reaction. *Chem. Mater.* **22**, 2178–2180 (2010).
88. J. Zhang, L. Dai, Heteroatom-doped graphitic carbon for efficient electrocatalysis of oxygen reduction reaction. *ACS Catal.,* in revision.
89. S. Wang, E. Iyyamperumal, A. Roy, Y. Xue, D. Yu, L. Dai, Vertically aligned BCN nanotubes as efficient metal-free electrocatalysts for the oxygen reduction reaction: A synergetic effect by co-doping with boron and nitrogen. *Angew. Chem. Int. Ed.* **50**, 11756–11760 (2011).
90. Y. Zhao, L. Yang, S. Chen, X. Wang, Y. Ma, Q. Wu, Y. Jiang, W. Qian, Z. Hu, Can boron and nitrogen co-doping improve oxygen reduction reaction activity of carbon nanotubes? *J. Am. Chem. Soc.* **135**, 1201–1204 (2013).
91. D. Yu, Y. Xue, L. Dai, Vertically aligned carbon nanotube arrays co-doped with phosphorus and nitrogen as efficient metal-free electrocatalysts for oxygen reduction. *J. Phys. Chem. Lett.* **3**, 2863–2870 (2012).
92. C. H. Choi, S. H. Park, S. I. Woo, Binary and ternary doping of nitrogen, boron, and phosphorus into carbon for enhancing electrochemical oxygen reduction activity. *ACS Nano* **6**, 7084–7091 (2012).
93. J. Xu, L. Guan, Toward understanding the active site for oxygen reduction reaction on phosphorus-encapsulated single-walled carbon nanotubes. *RSC Adv.* **3**, 5577–5582 (2013).
94. L. Zhang, Z. Xia, Mechanisms of oxygen reduction reaction on nitrogen-doped graphene for fuel cells. *J. Phys. Chem. C* **115**, 11170–11176 (2011).
95. L. Dai, Functionalization of graphene for efficient energy conversion and storage. *Acc. Chem. Res.* **46**, 31–42 (2013).
96. Q. Tang, Z. Zhou, Z. Chen, Graphene-related nanomaterials: Tuning properties by functionalization. *Nanoscale* **5**, 4541–4583 (2013).
97. K. S. Novoselov, V. I. Fal'ko, L. Colombo, P. R. Gellert, M. G. Schwab, K. Kim, A roadmap for graphene. *Nature* **490**, 192–200 (2012).
98. D. Deng, X. Pan, L. Yu, Y. Cui, Y. Jiang, J. Qi, W.-X. Li, Q. Fu, X. Ma, Q. Xue, G. Sun, X. Bao, Toward N-doped graphene via solvothermal synthesis. *Chem. Mater.* **23**, 1188–1193 (2011).
99. L. Feng, Y. Chen, L. Chen, Easy-to-operate and low-temperature synthesis of gram-scale nitrogen-doped graphene and its application as cathode catalyst in microbial fuel cells. *ACS Nano* **5**, 9611–9618 (2011).
100. Y. Zheng, J. Liu, J. Liang, M. Jaroniec, S. Z. Qiao, Graphitic carbon nitride materials: Controllable synthesis and applications in fuel cells and photocatalysis. *Energy Environ. Sci.* **5**, 6717–6731 (2012).
101. Y. Zheng, Y. Jiao, M. Jaroniec, Y. Jin, S. Z. Qiao, Nanostructured metal-free electrochemical catalysts for highly efficient oxygen reduction. *Small* **8**, 3550–3566 (2012).
102. X. Wang, K. Maeda, A. Thomas, K. Takanabe, G. Xin, J. M. Carlsson, K. Domen, M. Antonietti, A metal-free polymeric photocatalyst for hydrogen production from water under visible light. *Nat. Mater.* **8**, 76–80 (2009).
103. A. Thomas, A. Fischer, F. Goettmann, M. Antonietti, J.-O. Müller, R. Schlögl, J. M. Carlsson, Graphitic carbon nitride materials: Variation of structure and morphology and their use as metal-free catalysts. *J. Mater. Chem.* **18**, 4893–4908 (2008).
104. A. Vinu, K. Ariga, T. Mori, T. Nakanishi, S. Hishita, D. Golberg, Y. Bando, Preparation and characterization of well-ordered hexagonal mesoporous carbon nitride. *Adv. Mater.* **17**, 1648 (2005).
105. V. N. Khabashesku, J. L. Zimmerman, J. L. Margrave, Powder synthesis and characterization of amorphous carbon nitride. *Chem. Mater.* **12**, 3264–3270 (2000).
106. S. M. Lyth, Y. Nabae, S. Moriya, S. Kuroki, M.-a. Kakimoto, J.-i. Ozaki, S. Miyata, Carbon nitride as a nonprecious catalyst for electrochemical oxygen reduction. *J. Phys. Chem. C* **113**, 20148–20151 (2009).
107. Y. Sun, C. Li, Y. Xu, H. Bai, Z. Yao, G. Shi, Chemically converted graphene as substrate for immobilizing and enhancing the activity of a polymeric catalyst. *Chem. Commun.* **46**, 4740–4742 (2010).
108. S. Yang, X. Feng, X. Wang, K. Müllen, Graphene-based carbon nitride nanosheets as efficient metal-free electrocatalysts for oxygen reduction reactions. *Angew. Chem. Int. Ed.* **50**, 5339–5343 (2011).
109. W. S. Hummers Jr., R. E. Offeman, Preparation of graphitic oxide. *J. Am. Chem. Soc.* **80**, 1339 (1958).
110. S. Park, R. S. Ruoff, Chemical methods for the production of graphenes. *Nat. Nanotechnol.* **4**, 217–224 (2009).
111. D. Geng, Y. Chen, Y. Chen, Y. Li, R. Li, X. Sun, S. Ye, S. Knights, High oxygen-reduction activity and durability of nitrogen-doped graphene. *Energy Environ. Sci.* **4**, 760–764 (2011).
112. Z.-H. Sheng, L. Shao, J.-J. Chen, W.-J. Bao, F.-B. Wang, X.-H. Xia, Catalyst-free synthesis of nitrogen-doped graphene via thermal annealing graphite oxide with melamine and its excellent electrocatalysis. *ACS Nano* **5**, 4350–4358 (2011).
113. L. Lai, J. R. Potts, D. Zhan, L. Wang, C. K. Poh, C. Tang, H. Gong, Z. Shen, J. Lin, R. S. Ruoff, Exploration of the active center structure of nitrogen-doped graphene-based catalysts for oxygen reduction reaction. *Energy Environ. Sci.* **5**, 7936–7942 (2012).
114. Z. Lin, G. H. Waller, Y. Liu, M. Liu, C.-p. Wong, 3D Nitrogen-doped graphene prepared by pyrolysis of graphene oxide with polypyrrole for electrocatalysis of oxygen reduction reaction. *Nano Energy* **2**, 241–248 (2013).
115. Z. Lin, G. Waller, Y. Liu, M. Liu, C.-P. Wong, Facile synthesis of nitrogen-doped graphene via pyrolysis of graphene oxide and urea, and its electrocatalytic activity toward the oxygen-reduction reaction. *Adv. Energy Mater.* **2**, 884–888 (2012).
116. Z.-W. Liu, F. Peng, H.-J. Wang, H. Yu, W.-X. Zheng, J. Yang, Phosphorus-doped graphite layers with high electrocatalytic activity for the O_2 reduction in an alkaline medium. *Angew. Chem. Int. Ed.* **50**, 3257–3261 (2011).
117. C. H. Choi, M. W. Chung, H. C. Kwon, S. H. Park, S. I. Woo, B, N- and P, N-doped graphene as highly active catalysts for oxygen reduction reactions in acidic media. *J. Mater. Chem. A* **1**, 3694–3699 (2013).
118. I.-Y. Jeon, D. Yu, S.-Y. Bae, H.-J. Choi, D. W. Chang, L. Dai, J.-B. Baek, Formation of large-area nitrogen-doped graphene film prepared from simple solution casting of edge-selectively functionalized graphite and its electrocatalytic activity. *Chem. Mater.* **23**, 3987–3992 (2011).
119. I.-Y. Jeon, Y.-R. Shin, G.-J. Sohn, H.-J. Choi, S.-Y. Bae, J. Mahmood, S.-M. Jung, J.-M. Seo, M.-J. Kim, D. Wook Chang, L. Dai, J.-B. Baek, Edge-carboxylated graphene nanosheets via ball milling. *Proc. Natl. Acad. Sci. U.S.A.* **109**, 5588–5593 (2012).
120. I.-Y. Jeon, H.-J. Choi, M. J. Ju, I. T. Choi, K. Lim, J. Ko, H. K. Kim, J. C. Kim, J.-J. Lee, D. Shin, S.-M. Jung, J.-M. Seo, M.-J. Kim, N. Park, L. Dai, J.-B. Baek, Direct nitrogen fixation at the edges of graphene nanoplatelets as efficient electrocatalysts for energy conversion. *Sci. Rep.* **3**, 2260 (2013).
121. T. Chen, L. Dai, Carbon nanomaterials for high-performance supercapacitors. *Mater. Today* **16**, 272–280 (2013).
122. F. Du, D. Yu, L. Dai, S. Ganguli, V. Varshney, A. K. Roy, Preparation of tunable 3D pillared carbon nanotube-graphene networks for high-performance capacitance. *Chem. Mater.* **23**, 4810–4816 (2011).
123. D. Yu, K. Goh, H. Wang, L. Wei, W. Jiang, Q. Zhang, L. Dai, Y. Chen, Scalable synthesis of hierarchically structured carbon nanotube–graphene fibres for capacitive energy storage. *Nat. Nanotechnol.* **9**, 555–562 (2014).
124. N. P. Wickramaratne, J. Xu, M. Wang, L. Zhu, L. Dai, M. Jaroniec, Nitrogen enriched porous carbon spheres: Attractive materials for supercapacitor electrodes and CO_2 adsorption. *Chem. Mater.* **26**, 2820–2828 (2014).
125. Y. Xue, D. Yu, L. Dai, R. Wang, D. Li, A. Roy, F. Lu, H. Chen, Y. Liu, J. Qu, Three-dimensional B,N-doped graphene foam as a metal-free catalyst for oxygen reduction reaction. *Phys. Chem. Chem. Phys.* **15**, 12220–12226 (2013).
126. J. Zhang, X. S. Zhao, On the configuration of supercapacitors for maximizing electrochemical performance. *ChemSusChem* **5**, 818–841 (2012).
127. D.-S. Yang, D. Bhattacharjya, S. Inamdar, J. Park, J.-S. Yu, Phosphorus-doped ordered mesoporous carbons with different lengths as efficient metal-free electrocatalysts for oxygen reduction reaction in alkaline media. *J. Am. Chem. Soc.* **134**, 16127–16130 (2012).
128. R. Silva, D. Voiry, M. Chhowalla, T. Asefa, Efficient metal-free electrocatalysts for oxygen reduction: Polyaniline-derived N- and O-doped mesoporous carbons. *J. Am. Chem. Soc.* **135**, 7823–7826 (2013).
129. Z. Liu, H. Nie, Z. Yang, J. Zhang, Z. Jin, Y. Lu, Z. Xiao, S. Huang, Sulfur–nitrogen co-doped three-dimensional carbon foams with hierarchical pore structures as efficient metal-free electrocatalysts for oxygen reduction reactions. *Nanoscale* **5**, 3283–3288 (2013).

130. Y. Li, W. Zhou, H. Wang, L. Xie, Y. Liang, F. Wei, J.-C. Idrobo, S. J. Pennycook, H. Dai, An oxygen reduction electrocatalyst based on carbon nanotube graphene complexes. *Nat. Nanotechnol.* **7**, 394–400 (2012).
131. K. Kwon, Y. J. Sa, J. Y. Cheon, S. H. Joo, Ordered mesoporous carbon nitrides with graphitic frameworks as metal-free, highly durable, methanol-tolerant oxygen reduction catalysts in an acidic medium. *Langmuir* **28**, 991–996 (2011).
132. A. Kraytsberg, Y. Ein-Eli, The impact of nano-scaled materials on advanced metal–air battery systems. *Nano Energy* **2**, 468–480 (2013).
133. M. Armand, J.-M. Tarascon, Building better batteries. *Nature* **451**, 652–657 (2008).
134. R. Black, B. Adams, L. F. Nazar, Non-aqueous and hybrid Li-O_2 batteries. *Adv. Energy Mater.* **2**, 801–815 (2012).
135. Y. Shao, F. Ding, J. Xiao, J. Zhang, W. Xu, S. Park, J.-G. Zhang, Y. Wang, J. Liu, Making Li-air batteries rechargeable: Material challenges. *Adv. Func. Mater.* **23**, 987–1004 (2013).
136. N.-S. Choi, Z. Chen, S. A. Freunberger, X. Ji, Y.-K. Sun, K. Amine, G. Yushin, L. F. Nazar, J. Cho, P. G. Bruce, Challenges facing lithium batteries and electrical double-layer capacitors. *Angew. Chem. Int. Ed.* **51**, 9994–10024 (2012).
137. K. M. Abraham, Z. Jiang, A polymer electrolyte-based rechargeable lithium/oxygen battery. *J. Electrochem. Soc.* **143**, 1–5 (1996).
138. R. E. Williford, J.-G. Zhang, Air electrode design for sustained high power operation of Li/air batteries. *J. Power Sources* **194**, 1164–1170 (2009).
139. A. Kraytsberg, Y. Ein-Eli, Review on Li–air batteries—Opportunities, limitations and perspective. *J. Power Sources* **196**, 886–893 (2011).
140. J. Read, Characterization of the lithium/oxygen organic electrolyte battery. *J. Electrochem. Soc.* **149**, A1190–A1195 (2002).
141. C. Tran, X.-Q. Yang, D. Qu, Investigation of the gas-diffusion-electrode used as lithium/air cathode in non-aqueous electrolyte and the importance of carbon material porosity. *J. Power Sources* **195**, 2057–2063 (2010).
142. X.-h. Yang, P. He, Y.-y. Xia, Preparation of mesocellular carbon foam and its application for lithium/oxygen battery. *Electrochem. Commun.* **11**, 1127–1130 (2009).
143. X. Lin, L. Zhou, T. Huang, A. Yu, Hierarchically porous honeycomb-like carbon as a lithium–oxygen electrode. *J. Mater. Chem. A* **1**, 1239–1245 (2013).
144. H.-D. Lim, K.-Y. Park, H. Song, E. Y. Jang, H. Gwon, J. Kim, Y. H. Kim, M. D. Lima, R. O. Robles, X. Lepró, R. H. Baughman, K. Kang, Enhanced power and rechargeability of a Li–O_2 battery based on a hierarchical-fibril CNT electrode. *Adv. Mater.* **25**, 1348–1352 (2013).
145. T. Zhang, H. Zhou, From Li–O_2 to Li–air batteries: Carbon nanotubes/ionic liquid gels with a tricontinuous passage of electrons, ions, and oxygen. *Angew. Chem. Int. Ed.* **51**, 11062–11067 (2012).
146. J. Xiao, D. Mei, X. Li, W. Xu, D. Wang, G. L. Graff, W. D. Bennett, Z. Nie, L. V. Saraf, I. A. Aksay, J. Liu, J.-G. Zhang, Hierarchically porous graphene as a lithium–air battery electrode. *Nano Lett.* **11**, 5071–5078 (2011).
147. O. Gerbig, R. Merkle, J. Maier, Electron and ion transport in Li_2O_2. *Adv. Mater.* **25**, 3129–3133 (2013).
148. Y. Chen, S. A. Freunberger, Z. Peng, O. Fontaine, P. G. Bruce, Charging a Li–O_2 battery using a redox mediator. *Nat. Chem.* **5**, 489–494 (2013).
149. L. Zhong, R. R. Mitchell, Y. Liu, B. M. Gallant, C. V. Thompson, J. Y. Huang, S. X. Mao, Y. Shao-Horn, In situ transmission electron microscopy observations of electrochemical oxidation of Li_2O_2. *Nano Lett.* **13**, 2209–2214 (2013).
150. M. M. Ottakam Thotiyl, S. A. Freunberger, Z. Peng, P. G. Bruce, The carbon electrode in nonaqueous Li-O_2 cells. *J. Am. Chem. Soc.* **135**, 494–500 (2013).
151. Y.-C. Lu, Y. Shao-Horn, Probing the reaction kinetics of the charge reactions of nonaqueous Li-O_2 batteries. *J. Phys. Chem. Lett.* **4**, 93–99 (2013).
152. W.-H. Ryu, T.-H. Yoon, S. H. Song, S. Jeon, Y.-J. Park, I.-D. Kim, Bifunctional composite catalysts using Co_3O_4 nanofibers immobilized on nonoxidized graphene nanoflakes for high-capacity and long-cycle Li-O_2 batteries. *Nano Lett.* **13**, 4190–4197 (2013).
153. S. H. Oh, L. F. Nazar, Oxide catalysts for rechargeable high-capacity Li–O_2 batteries. *Adv. Energy Mater.* **2**, 903–910 (2012).
154. F. Li, T. Zhang, H. Zhou, Challenges of non-aqueous Li-O_2 batteries: Electrolytes, catalysts, and anodes. *Energy Environ. Sci.* **6**, 1125–1141 (2013).
155. J. Shui, F. Du, C. Xue, Q. Li, L. Dai, Vertically aligned N-doped coral-like carbon fiber arrays as efficient air electrodes for high-performance nonaqueous Li-O_2 batteries. *ACS Nano* **8**, 3015–3022 (2014).
156. K. Sakaushi, T.-P. Fellinger, M. Antonietti, Bifunctional metal-free catalysis of mesoporous noble carbons for oxygen reduction and evolution reactions. *ChemSusChem* **8**, 1156–1160 (2015).
157. J.-S. Lee, S. Tai Kim, R. Cao, N.-S. Choi, M. Liu, K. T. Lee, J. Cho, Metal–air batteries with high energy density: Li–air versus Zn–air. *Adv. Energy Mater.* **1**, 34–50 (2011).
158. E. Yoo, J. Nakamura, H. Zhou, N-Doped graphene nanosheets for Li–air fuel cells under acidic conditions. *Energy Environ. Sci.* **5**, 6928–6932 (2012).
159. E. Yoo, H. Zhou, Li–air rechargeable battery based on metal-free graphene nanosheet catalysts. *ACS Nano* **5**, 3020–3026 (2011).
160. R. Cao, R. Thapa, H. Kim, X. Xu, M. Gyu Kim, Q. Li, N. Park, M. Liu, J. Cho, Promotion of oxygen reduction by a bio-inspired tethered iron phthalocyanine carbon nanotube-based catalyst. *Nat. Commun.* **4**, 2076 (2013).
161. S. Zhu, Z. Chen, B. Li, D. Higgins, H. Wang, H. Li, Z. Chen, Nitrogen-doped carbon nanotubes as air cathode catalysts in zinc-air battery. *Electrochim. Acta* **56**, 5080–5084 (2011).
162. G. S. Park, J.-S. Lee, S. T. Kim, S. Park, J. Cho, Porous nitrogen doped carbon fiber with churros morphology derived from electrospun bicomponent polymer as highly efficient electrocatalyst for Zn–air batteries. *J. Power Sources* **243**, 267–273 (2013).
163. Y. Gorlin, T. F. Jaramillo, A bifunctional nonprecious metal catalyst for oxygen reduction and water oxidation. *J. Am. Chem. Soc.* **132**, 13612–13614 (2010).
164. F. Cheng, J. Shen, B. Peng, Y. Pan, Z. Tao, J. Chen, Rapid room-temperature synthesis of nanocrystalline spinels as oxygen reduction and evolution electrocatalysts. *Nat. Chem.* **3**, 79–84 (2011).
165. Z. Chen, A. Yu, D. Higgins, H. Li, H. Wang, Z. Chen, Highly active and durable core–corona structured bifunctional catalyst for rechargeable metal-air battery application. *Nano Lett.* **12**, 1946–1952 (2012).
166. B. Li, D. Geng, X. S. Lee, X. Ge, J. Chai, Z. Wang, J. Zhang, Z. Liu, T. S. A. Hor, Y. Zong, Eggplant-derived microporous carbon sheets: Towards mass production of efficient bifunctional oxygen electrocatalysts at low cost for rechargeable Zn–air batteries. *Chem. Commun.* **51**, 8841–8844 (2015).
167. L. Pan, G. Yu, D. Zhai, H. R. Lee, W. Zhao, N. Liu, H. Wang, B. C.-K. Tee, Y. Shi, Y. Cui, Z. Bao, Hierarchical nanostructured conducting polymer hydrogel with high electrochemical activity. *Proc. Natl. Acad. Sci. U.S.A.* **109**, 9287–9292 (2012).
168. G. Du, X. Liu, Y. Zong, T. S. A. Hor, A. Yu, Z. Liu, Co_3O_4 nanoparticle-modified MnO_2 nanotube bifunctional oxygen cathode catalysts for rechargeable zinc–air batteries. *Nanoscale* **5**, 4657–4661 (2013).
169. M. Prabu, P. Ramakrishnan, S. Shanmugam, $CoMn_2O_4$ nanoparticles anchored on nitrogen-doped graphene nanosheets as bifunctional electrocatalyst for rechargeable zinc–air battery. *Electrochem. Commun.* **41**, 59–63 (2014).
170. C. Sun, F. Li, C. Ma, Y. Wang, Y. Ren, W. Yang, Z. Ma, J. Li, Y. Chen, Y. Kim, L. Chen, Graphene–Co_3O_4 nanocomposite as an efficient bifunctional catalyst for lithium–air batteries. *J. Mater. Chem. A* **2**, 7188–7196 (2014).
171. J. K. Nørskov, J. Rossmeisl, A. Logadottir, L. Lindqvist, J. R. Kitchin, T. Bligaard, H. Jónsson, Origin of the overpotential for oxygen reduction at a fuel-cell cathode. *J. Phys. Chem. B* **108**, 17886–17892 (2004).
172. I. C. Man, H.-Y. Su, F. Calle-Vallejo, H. A. Hansen, J. I. Martínez, N. G. Inoglu, J. Kitchin, T. F. Jaramillo, J. K. Nørskov, J. Rossmeisl, Universality in oxygen evolution electrocatalysis on oxide surfaces. *ChemCatChem* **3**, 1159–1165 (2011).
173. W. A. Saidi, Oxygen reduction electrocatalysis using N-doped graphene quantum-dots. *J. Phys. Chem. Lett.* **4**, 4160–4165 (2013).
174. M. Li, L. Zhang, Q. Xu, J. Niu, Z. Xia, N-doped graphene as catalysts for oxygen reduction and oxygen evolution reactions: Theoretical considerations. *J. Catal.* **314**, 66–72 (2014).
175. Y. Jiao, Y. Zheng, M. Jaroniec, S. Z. Qiao, Origin of the electrocatalytic oxygen reduction activity of graphene-based catalysts: A roadmap to achieve the best performance. *J. Am. Chem. Soc.* **136**, 4394–4403 (2014).

Acknowledgments: We thank our colleagues for their contributions to the work cited. **Funding:** We are also grateful for financial support from NSF (CMMI-1400274, CMMI-1266295, AIR-IIP-1343270, DMR-1106160), DOD-AFOSR-MURI (FA9550-12-1-0037), and AFRL/DAGSI (RQ20-CWRU-13-4). **Author contributions:** J.Z. and L.D. conceived and prepared the manuscript. J.Z. performed electrochemical studies. Z.X. and L.D. revised the manuscript. All authors commented on the manuscript. **Competing interests:** The authors declare that they have no competing interests.

Submitted 5 May 2015
Accepted 20 July 2015
Published 28 August 2015
10.1126/sciadv.1500564

Citation: J. Zhang, Z. Xia, L. Dai, Carbon-based electrocatalysts for advanced energy conversion and storage. *Sci. Adv.* **1**, e1500564 (2015).